Center for Environmentally Sustainable Transportation in Cold Climates

Environmentally Friendly Pervious Concrete for Treating Deicer-Laden Stormwater (Phase II Report)

Gang Xu, M.Sc., P.E.
Xianming Shi, Ph.D., P.E.
Department of Civil and Environmental Engineering
Washington State University

Date: 12/31/2018

Prepared by: Gang Xu and Xianming Shi

Center for Environmentally Sustainable Transportation in Cold Climates
University of Alaska Fairbanks
P.O. Box 755900
Fairbanks, AK 99775

U.S. Department of Transportation
1200 New Jersey Avenue, SE
Washington, DC 20590

INE/CESTiCC 18.12

Environmentally Friendly Pervious Concrete for Treating Deicer-Laden Stormwater

(Phase II Report)

by

Gang Xu, M.Sc., P.E.

Xianming Shi, Ph.D., P.E.

Department of Civil and Environmental Engineering
Washington State University

INE/AUTC 18.12

December 2018

REPORT DOCUMENTATION PAGE	Form approved OMB No.

1. AGENCY USE ONLY (LEAVE BLANK)	2. REPORT DATE	3. REPORT TYPE AND DATES COVERED
	7/2018	Final Report: 8/2016 – 7122018

4. TITLE AND SUBTITLE

Environmentally Friendly Pervious Concrete for Treating Deicer-Laden Stormwater (Phase II Final Report)

5. FUNDING NUMBERS

6. AUTHOR(S)

Gang Xu, M.Sc., P.E.
Xianming Shi, Ph.D., P.E.
Department of Civil and Environmental Engineering, Washington State University

7. PERFORMING ORGANIZATION NAME(S) AND ADDRESS(ES)

Laboratory of Advanced & Sustainable Cementitious Materials
Washington State University
405 Spokane Street, Sloan 101, P.O. Box 755900
Pullman, WA 99164

8. PERFORMING ORGANIZATION REPORT NUMBER

INE/AUTC 18.12

9. SPONSORING/MONITORING AGENCY NAME(S) AND ADDRESS(ES)

U.S. Department of Transportation
1200 New Jersey Avenue, SE
Washington, DC 20590

10. SPONSORING/MONITORING AGENCY REPORT NUMBER

11. SUPPLENMENTARY NOTES

12a. DISTRIBUTION / AVAILABILITY STATEMENT

No restrictions

12b. DISTRIBUTION CODE

13. ABSTRACT (Maximum 200 words)

In Phase I of this project, graphene oxide (GO)-modified pervious concrete was developed using coal fly ash as the sole binder. The primary objectives of Phase II of this project were (1) to evaluate the stormwater infiltration capacity of GO-modified fly ash pervious concrete; (2) to evaluate the durability performance of GO-modified fly ash pervious concrete using freeze/thaw and salt resistance testing methods; and (3) to use advanced analytical tools to fully characterize the GO-modified fly ash binder. Test results indicate different degrees of reduction in concentrations of possible pollutants in stormwater—copper, zinc, sulphate, chloride, ammonia, nitrate, and total phosphate. The incorporation of GO significantly improved the resistance of pervious concrete to freeze/thaw cycles and ambient-temperature salt attack. The specimens were examined using X-ray diffraction, which revealed that the mineralogy and the chemical composition of fly ash pastes differ considerably from those of cement pastes. Nuclear magnetic resonance was used to study the chemical structure and ordering of different hydrates, and provided enhanced understanding of the freeze/thaw and salt scaling resistance of fly ash pervious concrete and the role of GO.

14. KEYWORDS:

Fly ash, pervious concrete, graphene oxide, NMR, XRD, stormwater

15. NUMBER OF PAGES

91

16. PRICE CODE

N/A

17. SECURITY CLASSIFICATION OF REPORT	18. SECURITY CLASSIFICATION OF THIS PAGE	19. SECURITY CLASSIFICATION OF ABSTRACT	20. LIMITATION OF ABSTRACT
Unclassified	Unclassified	Unclassified	N/A

NSN 7540-01-280-5500

STANDARD FORM 298 (Rev. 2-98)
Prescribed by ANSI Std. 239-18 2

DISCLAIMER

This document is disseminated under the sponsorship of the U.S. Department of Transportation in the interest of information exchange. The U.S. Government assumes no liability for the use of the information contained in this document. The U.S. Government does not endorse products or manufacturers. Trademarks or manufacturers' names appear in this report only because they are considered essential to the objective of the document.

Opinions and conclusions expressed or implied in the report are those of the author(s). They are not necessarily those of the funding agencies.

METRIC (SI*) CONVERSION FACTORS

APPROXIMATE CONVERSIONS TO SI UNITS

Symbol	When You Know	Multiply By	To Find	Symbol
		LENGTH		
in	inches	25.4		mm
ft	feet	0.3048		m
yd	yards	0.914		m
mi	Miles (statute)	1.61		km
		AREA		
in^2	square inches	645.2	millimeters squared	cm^2
ft^2	square feet	0.0929	meters squared	m^2
yd^2	square yards	0.836	meters squared	m^2
mi^2	square miles	2.59	kilometers squared	km^2
ac	acres	0.4046	hectares	ha
		MASS (weight)		
oz	Ounces (avdp)	28.35	grams	g
lb	Pounds (avdp)	0.454	kilograms	kg
T	Short tons (2000 lb)	0.907	megagrams	mg
		VOLUME		
fl oz	fluid ounces (US)	29.57	milliliters	mL
gal	Gallons (liq)	3.785	liters	liters
ft^3	cubic feet	0.0283	meters cubed	m^3
yd^3	cubic yards	0.765	meters cubed	m^3

Note: Volumes greater than 1000 L shall be shown in m^3

		TEMPERATURE (exact)		
ºF	Fahrenheit	5/9 (ºF-32) ºC temperature temperature	Celsius	
		ILLUMINATION		
fc	Foot-candles	10.76	lux	lx
fl	foot-lamberts	3.426	candela/m^2	cd/cm^2
		FORCE and PRESSURE or STRESS		
lbf	pound-force	4.45	newtons	N
psi	pound-force per square inch	6.89	kilopascals	kPa

These factors conform to the requirement of FHWA Order 5190.1A *SI is the symbol for the International System of Measurements

APPROXIMATE CONVERSIONS FROM SI UNITS

Symbol	When You Know	Multiply By	To Find	Symbol
		LENGTH		
mm	millimeters	0.039	inches	in
m	meters	3.28	feet	ft
m	meters	1.09	yards	yd
km	kilometers	0.621	Miles (statute)	mi
		AREA		
mm^2	millimeters squared	0.0016	square inches	in^2 m^2
meters squared		10.764	square feet	ft^2 km^2
kilometers squared		0.39	square miles	mi^2 ha
hectares (10,000 m^2)		2.471	acres	ac
		MASS (weight)		
g	grams	0.0353	Ounces (avdp)	oz
kg	kilograms	2.205	Pounds (avdp)	lb mg
megagrams (1000 kg)		1.103	short tons	T
		VOLUME		
mL	milliliters	0.034	fluid ounces (US)	fl oz
liters		0.264	Gallons (liq)	gal
m^3	meters cubed	35.315	cubic feet	ft^3
m^3	meters cubed	1.308	cubic yards	yd^3
		TEMPERATURE (exact)		
ºC	Celsius temperature	9/5 ºC+32	Fahrenheit temperature	ºF
		ILLUMINATION		
lx	lux	0.0929	foot-candles	fc
cd/cm ^{2}	candela/m^2	0.2919	foot-lamberts	fl
		FORCE and PRESSURE or STRESS		
N	newtons	0.225	pound-force	lbf
kPa	kilopascals	0.145	pound-force per square inch	psi

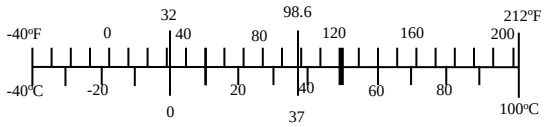

ACKNOWLEDGMENTS

The authors would like to thank the Center for Environmentally Sustainable Transportation in Cold Climates (CESTiCC) for funding this work. They also would like to thank faculty, staff, and students from the Laboratory of Advanced & Sustainable Cementitious Materials, Peter Hooper GeoAnalytical Lab and Composite Materials & Engineering Center at Washington State University. The authors appreciate the cooperation from Montana State University.

TABLE OF CONTENTS

LIST OF FIGURES

LIST OF TABLES

EXECUTIVE SUMMARY

In Phase I of this project, graphene oxide (GO)-modified pervious concrete was developed using coal fly ash as the sole binder. The primary objectives of Phase II of this project were (1) to evaluate the stormwater infiltration capacity of GO-modified fly ash pervious concrete; (2) to evaluate the durability performance of GO-modified fly ash pervious concrete using freeze/thaw and salt resistance testing methods; and (3) to use advanced analytical tools to fully characterize the GO-modified fly ash binder.

Following the Phase I research, the freeze/thaw (F/T) resistance and the ambient-temperature salt resistance of pervious concrete specimens were investigated separately, to isolate the physical and chemical phenomena underlying their deterioration during the "salt scaling" test, which combined the effects of F/T cycling and deicer attack. Test results suggest that the incorporation of GO can significantly improve resistance to F/T, ambient-temperature salt attack, and "salt scaling" of pervious concrete, for both the cement and activated fly ash binder. During the salt scaling test, GO-modified fly ash pervious concrete specimens exhibited the least weight loss. This result is partly attributable to the GO-modified hydration products of fly ash, which have better resistance than conventional cement hydrates. The specimens were studied using X-ray diffraction and secondary electron imaging tools. Nuclear magnetic resonance was also employed to examine the degree of polymerization of hydrates. This study

provides enhanced understanding of the F/T and salt scaling resistance of fly ash pervious concrete with or without GO modification.

CHAPTER 1.0 INTRODUCTION

1.1 Background

Pervious concrete is a special type of concrete; its high porosity allows water from precipitation and other sources to pass through directly (Fig. 1.1). The infiltration effect provided by pervious concrete pavement not only recharges groundwater, but also reduces the amount of total suspended solids, total phosphor, total nitrogen, and metals in groundwater (Schaefer et al. 2006a). In addition, pervious concrete meets U.S. Environmental Protection Agency (EPA) stormwater regulations.

Figure 1.1 Pervious concrete demonstration (photo by J.J. Harrison)

One study (Dierkes et al. 2000) provided the concentrations of possible pollutants in rain: copper (1–355 μg/l), zinc (5–235 μg/l), sulphate (0.56–14.40 mg/l), chloride (0.2–5.2 mg/l), ammonia (0.1–2.0 mg/l), nitrate (0.l–7.4 mg/l), total phosphate (0.01–0.19 mg/l), and 5-day biochemical oxygen demand (1–2 mg/l). Another study (Lee et al. 2014) evaluated the ability of pervious concrete to remove pollutant concentrations. The study results showed that pervious concrete effectively reduced pollutant concentrations in diluted sulfuric acid (pH value 2.0 was increased to approximately 7.0), artificial seawater (salinity was reduced from 36% to about 1%), and motor oil tests. Horner et al. (1994) performed chemical analyses of rainfall samples after rainwater passed through pervious concrete pavement. The concentrations of metals in collected samples were found low, substantially below the nationwide average; total petroleum hydrocarbons were not detected in any samples. Pervious concrete shows promise as an effective

means of addressing the deicer-laden stormwater issue in cold regions, thus supporting environmental conservation.

Numerous studies have focused on the environmental benefits of cement-based pervious concrete materials (Azfar 2009, Joung 2008, Marchand et al. 1999). The GO-modified fly ash pervious concrete developed in Phase I of the present research required further study. Since fly ash binder is fundamentally different from cement binder, the Phase II investigation set out to determine the water treatment effectiveness of GO-modified fly ash pervious concrete and to address concerns about heavy metal leaching from the fly ash itself.

The recent development of nanosize materials presents an opportunity to improve the overall performance of pervious concrete materials. Among numerous nanomaterials, graphene oxide (GO) shows potential as an admixture for concrete because it is a two-dimensional carbon sheet with an aspect ratio of 30,000 or higher (Tung et al. 2009), has a Young's modulus of 1 TPa and an intrinsic strength of 130 Gpa, and is highly hydrophilic (Lee et al. 2008). Using scanning electron microscopy (SEM), Lv et al. (2014) observed that different amounts of GO (0.01–0.06% by weight of cement) promoted flower-like and polyhedron-like cement hydration products (Fig. 1.2) that formed a compact microstructure. As a result, the flexural strength and compressive strength of cement mix with 0.03% GO were considerably improved—by 60.7% and 38.9%, respectively. Graphene oxide also demonstrated a crack deflection or branching mechanism, which increases a crack path to release stress in cement paste.

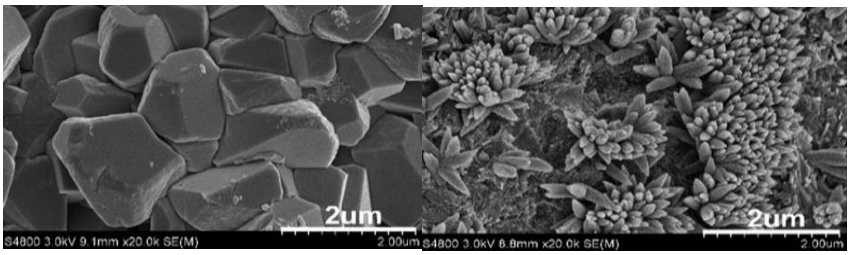

Figure 1.2 SEM image of cement hydrates at 7- days: ~~(top)~~ flower-like shape (right); ~~(bottom)~~ polyhedron-like shape (left) (Lv et al. 2014)

During our Phase I study, the beneficial use of GO in fly ash pervious concrete material was explored. The results suggest that GO can significantly improve the overall performance of fly ash pervious concrete by increasing the degree of polymerization and the average bulk Ca/Si ratio of fly ash hydration products (Fig. 1.3).

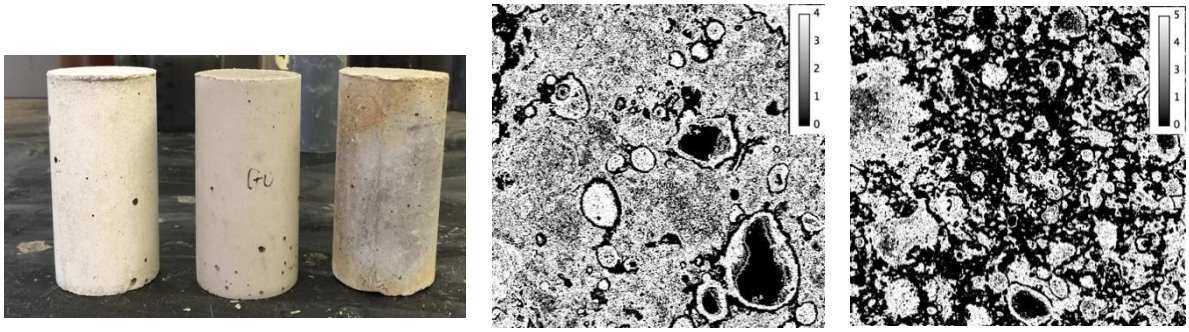

Figure 1.3 GO-modified fly ash mortar surface comparison (left); Ca/Si mole ratio mapping of regular fly ash mortar (middle); GO-modified fly ash mortar (right)

Durability tests were also performed to evaluate the Phase I GO-modified pervious concrete. The degradation test indicated that GO-modified fly ash pervious concrete degradation resistance is comparable to that of cement pervious concrete at 90 days according to ASTM C1747. The freeze-deicer salt scaling test conducted at 28 days, however, suggested that the initial weight loss of GO-modified fly ash pervious concrete is higher than that of cement pervious concrete due to the slow hydration of fly ash. Mechanical or chemical techniques can be used to improve the early-age performance of GO-modified fly ash pervious concrete.

The technology developed in Phase I showed great potential for biomass ash solidification. Biomass ash is produced from burning wood chips, bark, straw, rice husks, etc. Since biomass is a renewable resource, its combustion essentially does not contribute to the greenhouse effect due to fast CO_2 conversion (Vassilev et al. 2013). The utilization of biomass energy as an alternative to fossil energy has increased rapidly in recent years. The global growth of biomass production is estimated to be 112–220 billion tonnes per year (Demirbas 2005, Williams et al. 2012). The oxide content of biomass ash is typically (in decreasing order) SiO_2 > CaO > K_2O > P_2O_5 > Al_2O_3 > MgO > Fe_2O_3 > SO_3 (Vassilev et al. 2013). The phase-mineral composition of biomass ash is mostly non-crystalline and crystalline to semi-crystalline, similar to fly ash. More than 425,000 metric tons of wheat straw is produced annually within 50 miles of Washington State University (WSU). This resource provided biomass ash for this project.

The Phase I technology developed for fly ash shows technological and environmental advantages related to biomass ash.

1.2 Problem Statement

Pervious concrete is a green concrete with many environmental benefits. Using fly ash in pervious concrete to treat deicer-laden stormwater is another environmental benefit, entitling this type of concrete to be considered environmentally friendly. As a by-product of coal-fired power plants, fly ash has been used as supplementary cementitious material (SCM) in concrete for years. However, it is typically used at a replacement rate of less than 35% by mass of cement due to the lack of understanding of its overall performance (Minkara 2015). One study (Berry et al. 2011) demonstrated the possibility of using fly ash as the sole cementitious binder in making concrete of moderate strength, provided the calcium content of fly ash is high enough. This fly

ash was recognized as *high-calcium, high-reactivity* fly ash (Enders 1995) in Phase I of the present research, and it is cementitious in nature.

Although most *high-calcium* fly ash shows *low-reactivity*, Phase I research successfully demonstrated that *high-calcium, low-reactivity* fly ash can act like self-cementitious material in the presence of water, chemical activators (sodium silicate, quicklime, calcium chloride, and sodium sulphate), and graphene oxide (GO), which forms a thick coating around aggregates and is able to replace 100% Portland cement in pervious concrete (Xu and Shi 2016) with moderate strength.

The research results from Phase I suggested the use of GO-modified fly ash pervious concrete in pavement applications and as deicer-laden stormwater treatment, but some areas related to its use still needed study and evaluation (Phase II).

1.2.1 Deicer-laden stormwater treatment and other environmental benefits

Deicer-laden stormwater treatment tests should be conducted to evaluate the effectiveness of filtration function provided by fly ash pervious concrete. Such tests could address concerns about heavy metal leaching from fly ash itself, which can cause water contamination (Sushil and Batra 2006). Since fly ash binder is fundamentally different from cement binder, other environmental benefits of fly ash pervious concrete, such as heat-island effects and acoustic absorption effects, also need evaluation.

1.2.2 Performance evaluation

One significant barrier to the implementation of pervious concrete pavement is its lack of durability in cold climates. Specifically, the use of chemical deicers in cold regions tends to exacerbate the susceptibility of concrete infrastructure to freeze/thaw (F/T) cycles (Anderson and Dewoolkar 2015, Shi et al. 2009, Valenza and Scherer 2007). Relative to impervious concrete,

pervious concrete is prone to the ingress of water and deicer solution and is thus more vulnerable to premature failure due to salt scaling damage. Previous studies (Amde and Rogge 2013; Yang et al. 2006) found that a characteristic of pervious concrete is weak resistance to F/T cycles.

In this Phase II project, the F/T resistance and ambient-temperature salt resistance of pervious concrete specimens were investigated separately, to isolate the physical and chemical phenomena underlying the deterioration of specimens during the "salt scaling" test, which combined the effects of F/T cycling and deicer attack. Sustainable pervious concrete with fly ash as the sole binder was developed with alkali activation at room temperature. Graphene oxide was used to facilitate the polymerization of reaction products from alkali activation. Studies by Lv et al. (2014), Gong et al. (2015), and Ranjbar et al. (2015) indicated that GO can substantially improve the overall performance of cement mix by regulating cement hydration, providing a mechanism for crack branching and bridging and acting as nanofillers. Therefore, GO has significant potential for application in fly ash-based pervious concrete of high strength and durability.

1.2.3 Characterization of fly ash binder

As just mentioned, studies by Gong et al. (2015), Lv et al. (2014), and Ranjbar et al. (2015) reported that GO can improve the overall performance of cement and geopolymer by regulating cement hydration, providing a crack branching and bridging mechanism and acting as nanofillers. However, currently no research to determine the function of GO in fly ash binder has been reported. More study is needed to characterize fly ash hydration products with GO. Advanced tools such as the analytical techniques of scanning electron microscopy (SEM), nuclear magnetic resonance (NMR), Fourier transform infrared spectroscopy (FTIR), X-ray

diffraction (XRD), and X-ray fluorescence (XRF) can be used to determine the chemical compositions, mineralogy, and degree of polymerization of hydrates,

Research is needed to advance our understanding of the GO-modified fly ash pervious concrete developed in Phase I of this research, especially since such concrete is intended for pavement applications.

1.3 Outline of Report

This report has five chapters. Chapter 1 outlines the scope of work. Chapter 2 provides a comprehensive literature review of the environmental benefits, durability, and characterization of fly ash concrete. Chapter 3 addresses the F/T test, deicer wet-dry cycle test, and stormwater infiltration test of fly ash pervious concrete. Chapter 4 includes a description and discussion of fly ash hydrates and the function of GO in the hydration system. Chapter 5 summarizes the work of this report and gives conclusions.

CHAPTER 2.0 LITERATURE REVIEW

2.1 Introduction

Recent years have seen many scientific advances in characterization and up-cycling technologies of fly ash, which in turn have significantly promoted the value-added applications of fly ash, for example, fly ash-based geopolymer, SCM, and zeolite synthesis. Typical utilizations of fly ash are presented in Fig. 2.1. Fly ash is also used in flowable fill, embankments, road base, blasting grit, catalysis, mining applications, waste stabilization, agriculture, and oil field service (Zhuang et al. 2016).

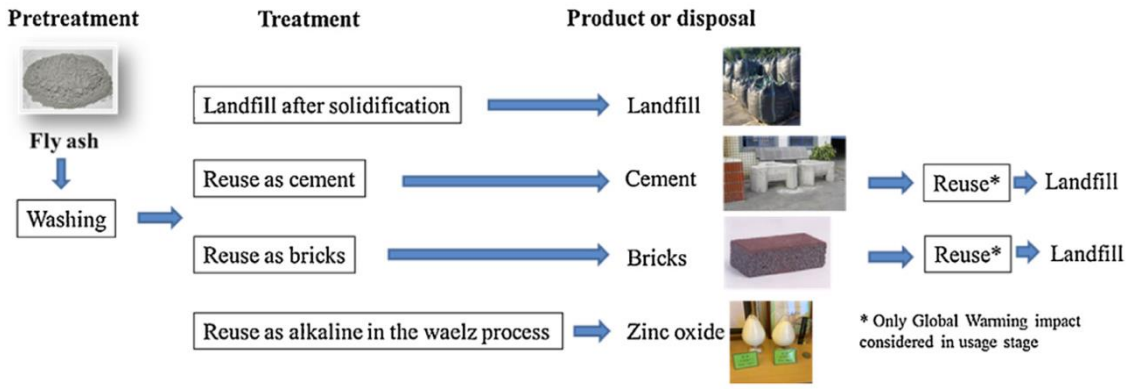

Figure 2.1 Scenarios for fly ash reuse (Huang et al. 2017a)

Information in the published domain since 2000 and from the fly ash up-cycling community was gathered and analyzed in depth, with a focus on recent advances in characterization, compositional understanding, and activation approaches. The authors identified important needs for future research to support the optimal and appropriate utilization of fly ash. The findings from this work will promote the beneficial use of fly ash as a component of a sustainable future construction material industry.

2.2 Fly Ash Characterization

Fly ash is an artificial volcanic material. The definition of volcanic fly ash is "silicate or aluminosilicate material, which possess weak or non-self-cementing ability, but in the finely divided state and damp environments at room temperature, it reacts with $Ca(OH)_2$ to form gel products" (Dunstan 1989). The physical and chemical characteristics of fly ash depend on coal type, boiler, operating conditions, and post-combustion conditions (Kutchko and Kim 2006). To characterize fly ash, XRD, XRF, FTIR, SEM/EDS (energy dispersive X-ray spectroscopy), and MAS (magic angle spinning)-NMR are often used. The following sections provide further discussion of fly ash in terms of physical, chemical, and mineralogical properties (Fig. 2.2).

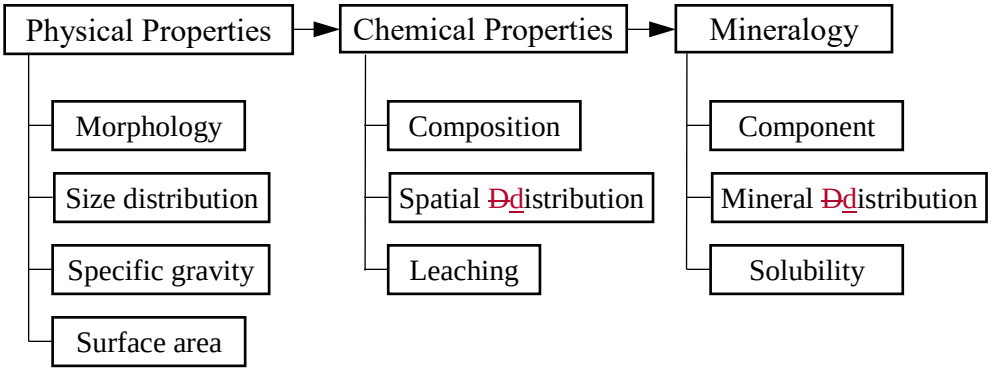

Figure 2.2 Schematic overview of fly ash characterization

2.3 Morphology and Physical Properties

Fly ash particles are mostly spherical in shape, including solid spheres (density = 2300–2600 kg/m^3) and cenospheres (0.2–1.1% of the total fly ash weight, density < 1400 kg/m^3) (Brouwers and Van Eijk 2002) (Fig. 2.3a,d). Fly ash also has irregular-shaped minerals and unburnt carbon (Fig. 2.3e,f). Depending on the source, fly ash particles vary in size, ranging from less than 1μm to greater than 200 μm, but hollow cenospheres and irregularly unburned carbon particles tend toward the upper end of the size distribution. Some ash may be finer or coarser than Portland cement particles (Brouwers and Van Eijk 2002, Ramezanianpour 2014).

High-calcium fly ash is typically finer than low-calcium fly ash, due to the presence of larger amounts of alkali sulphate in high-calcium fly ash (Mehta 1984). Granulometry distribution of five fly ash samples, obtained by laser ray diffraction, is shown in Fig. 2.4.

The morphology of fly ash particles is mainly controlled by combustion temperature, cooling rate, and the composition of particles. For instance, spherical particles in fluidized bed combustion ash are rarely observed, and most of the particles exhibit irregular shapes (Fig.2.3b). Seo et al. (2010) and Stutzxnan and Centeno (1995) thought that most minerals in the FBC (fluidized bed combustion) ash do not undergo melting but soften only, under the relatively low boiler temperature of 850-900°C of the FBC method. Most high-calcium ashes are spheres owing to the low melting point of Ca-modified ash. The Brunauer-Emmett-Teller analysis and Blaine air permeability test are often adopted to measure the specific surface area of fly ash, which varies from 150 m^2/kg for mechanically collected fly ash to 1200 m^2/kg for fly ash collected by electrostatic precipitators (Mehta 1984). The specific gravity of fly ash varies from a low value of 1.90 for a subbituminous ash, to a high value of 2.96 for an iron-rich bituminous ash (Mehta 1984).

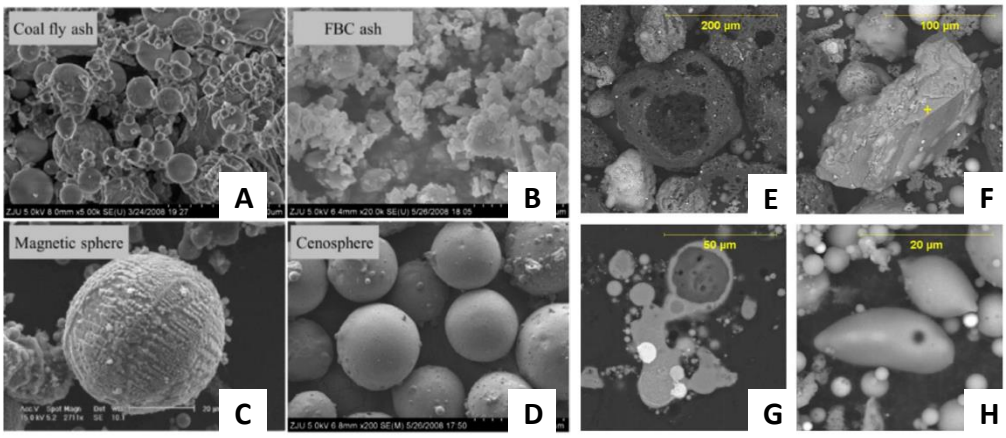

Figure 2.3 Fly ash particles: (a) sphere; (b) FBC ash; (c) magnetic sphere; (d) cenosphere; (e) carbon particle; (f) mineral aggregate; (g) agglomerated particles; (h) irregularly shaped particles. (Kutchko and Kim 2006; Yao et al. 2015)

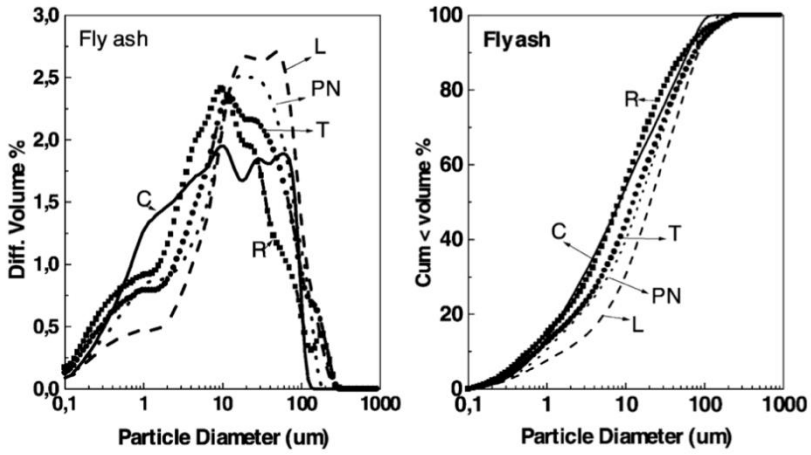

Figure 2.4 Granulometry distribution of fly ash (C, L, and PN are ashes with high SiO_2/Al_2O_3 ratio ≈ 2%; R and T have high amounts of Fe_2O_3) (Fernández-Jiménez and Palomo 2003).

2.4 Chemical Compositions

The main chemical composition of fly ash is aluminosilicate compounds (Iribarne et al. 2001); fly ash also contains some metallic and calcium oxides (Brouwers and Eijk 2003). The contents of principal oxides are SiO_2 (20–65 wt%), Al_2O_3 (4–20 wt%), Fe_2O_3 (4–20 wt%), CaO (< 30 wt%), MgO (1–5 wt%), K_2O, Na_2O (total alkalis < 8 wt%), and SO_3 (<12 wt%), and loss on ignition (LOI) is usually less than 5 wt% (Ramezanianpour 2014). Enders (1995) found that the ratio of $A1_2O_3/(A1_2O_3 + SiO_2)$ in fly ash spheres can be constant, indicating the origin of glassy spheres from kaolinite in coal. Fly ash contains many trace elements, such as Cr, Pb, Ni, Ba, Sr, V, and Zn (Yao et al. 2015), which are typically enriched in magnetospheres (Yang et al. 2014). Vassilev et al. (2004b) showed that the water-soluble content (0.2–0.6 wt%) of fly ash was abundant in S and Ca, to a lesser extent in Al, Si, Na, K, Mg, Cl, Fe, P, and Ti, and includes trace elements of Cs, Li, Mn, Ni, Sn, and Sr at the ppm level, and As, Ba, Cr, Cu, Ge, Mo, Pb, Rb, Sb, Se, V, Zn, and Zr at the ppb level. Their analysis showed that 2–29 wt% of Ca, Cl, Na, and S, and 0.1–1 wt% of Al, Cs, K, Mg, P, Si, Sn, and Ti were able to leach from the initial

elemental contents of fly ash (Vassilev et al. 2004b). Sulphate concentrations in pore solutions of fly ash-water pastes were found to rise significantly between 7 and 90 days, but this increase could be a short-term phenomenon (Tishmack et al. 2001). Due to the fixation of heavy metals in hydrated phases, the concentration of some heavy metals in the solution decreases with the development of fly ash hydration (Ubbrìaco et al. 2001).

Based on the CaO content, fly ash can be divided into high-calcium fly ash (CaO content > 10 wt%) and low-calcium fly ash (CaO Content < 10 wt%) (Fan et al. 2015). In accordance with ASTM C618, high-calcium fly ash is produced from burning lignite, sub-bituminous coal, since lignite, sub-bituminous coal, has a high CaO content, up to 10 wt%. Low-calcium fly ash typically is produced by combustion of anthracite, bituminous coal. Fly ash with (SiO_2 + Al_2O_3+ Fe_2O_3) > 70 wt% is classified as Class F ash. Fly ash with 70 wt% > (SiO_2+ Al_2O_3+ Fe_2O_3) > 50 wt% is classified as Class C fly ash (C09 Committee 2012).

Low-calcium fly ash has been widely used as a geopolymer admixture or as an admixture of concrete, and has demonstrated very good performance (Bae et al. 2014, Lee et al. 2003, Li et al. 2010, Palomo et al. 1999, Yao et al. 2015). Gress (1997) suggested that high-calcium fly ash may contribute to premature distress in concrete. One of the mechanisms of concrete deterioration identified was distress caused by delayed ettringite formation from high-calcium ash (Tishmack et al. 1999). The high content of free lime, which leads to cement instability, is a major concern hindering its utilization. However, recent years have seen increasing use of younger lignite or sub-bituminous coal at power plants, which has led to an increase in the availability of high-calcium fly ash (Li 2011). This renders research imperative to better recycle and utilize the high-calcium fly ash.

Calcium content is also an important factor associated with fly ash cementitious properties. Fracture of the outer shell of ash particles is important in the hydration process, since it makes CaO in the core of these particles available for further reaction. Higher contents of SO_3 were found beneficial to the self-cementitious strength of fly ash (Illikainen et al. 2014, Sheng et al. 2007). Table 2.1 shows that the heating and cooling condition is another essential factor associated with the pozzolanic or cementitious properties of fly ash, which determine the composition and morphology of fly ash particles (Kutchko and Kim 2006).

Table 2.1 Factors determining cementitious or pozzolanic properties of fly ash

	Cementitious Ash	**Pozzolanic Ash**
Production Methods	1. Dry process flue gas desulphurization [FGD] by-products (McCarthy and Solem-Tishmack 1994) 2. Clean coal technology by-products that use lime as a sorbent (McCarthy and Solem-Tishmack 1994; Sheng et al. 2012; Šiler et al. 2015)	1. Wet process FGD by-products (McCarthy and Solem-Tishmack 1994) 2. Bottom ash slags (McCarthy and Solem-Tishmack 1994)
Calcium Content	Calcium content > 20 wt.% (McCarthy and Solem-Tishmack 1994)	Calcium content < 20 wt.% (McCarthy and Solem-Tishmack 1994)
Temperature	Given the same other conditions, a higher temperature generally tends to produce cementitious ash, such as a pulverized coal-fired boiler at temperature > 1400ºC (Kutchko and Kim 2006; Song et al. 2015),	Given the same other conditions, a lower temperature generally tends to produce pozzolanic ash, such as FBC at temperature (800–1000ºC) (Iribarne et al. 2001)

2.5 Mineralogical Compositions

Approximately 316 individual minerals and 188 mineral groups have been identified in fly ash (Vassilev 2003, Vassilev and Vassileva 2005, Vassilev et al. 2004a,b, Vassilev et al. 2005). The content of crystalline minerals is in the range of 11 to 48 wt% (Li 2011). The mineral composition of high-calcium fly ash, which has larger amounts of crystalline CaO (1–2.5 wt%), C_3A (48 wt%), and C_4A_3S (1–2.5 wt%), is generally more complex than low-calcium fly ash

(McCarthy and Solem-Tishmack 1994). Table 2.2 summarizes the mineral contents in the case of different groups.

Table 2.2 Common phase-mineral content in fly ash (Li 2011; Vassilev et al. 2004b; Velandia et al. 2016)

Low-calcium fly ash	Anhydrite ($CaSO_4$), Coesite (SiO_2), Hematite (Fe_2O_3), Mullite ($2Al_2O_3.2SiO_2$), Quartz (SiO_2), Magnesioferrite ($Mg(Fe)_2O_4$), Magnetite (Fe_3O_4).
High-calcium fly ash	Akermanite (Ca, Mg, Al (Si_2O_7)), Anhydrite ($CaSO_4$), $C_4A_3\bar{S}$ ($Ca_4Al_6(SO_4)O_{12}$), Cristobalite (SiO_2), Feldspar (Na, Ca, Al) silicate, Ferrite – spinel ((Mg, Fe)(Fe, $Mg)_2O_4$), Lime (CaO), Merwinite ($Ca_3Mg(SiO_4)_2$), Periclase (MgO), Quartz, Tetracalcium aluminoferrite ($Ca_4Al_2Fe_2O_{10}$), Tricalcium aluminate ($Ca_3Al_2O_6$), Tricalcium silicate (Ca_3SiO_5), Wollastonite (Ca_2SiO_4).
Cenosphere	Amorphous glass (SiO_2), Calcite ($CaCO_3$), Cristobalite, Dolomite ($CaMg(CO_3)_2$), Fe-oxides, Gypsum ($CaSO_4$), K-feldspar, Mullite ($Al_6Si_2O_{13}$), Plagioclase ($NaAlSi_3O_8$-$CaAl_2Si_2O_8$), Quartz.
Water-soluble minerals of fly ash	Alunite ($KAl_3(SO_4)_2(OH)_6$), Anhydrite, Ankerite ($Ca(Fe,Mg,Mn)(CO_3)_2$), Bassanite ($CaSO_4{\cdot}0.5(H_2O)$), Calcite, Dolomite, Gypsum, Halite (NaCl), Jarosite ($KFe_3(OH)_6(SO_4)_2$), Opal ($SiO_2{\cdot}nH_2O$), Zeolite.

Quartz and mullite are main crystalline phases in fly ash (Velandia et al. 2016). Quartz typically is not reactive during fly ash hydration. The content of quartz varies from 4–23 wt% in different ashes (Ramezanianpour 2014, Velandia et al. 2016). Quartz of large crystallite size (> 125 nm) and pure composition is primarily from coal, and is called primary quartz (Fig. 2.5a). The quartz of smaller crystallite size (< 125 nm), higher atomic displacement parameters (increased disorder), and larger lattice parameters (substitution by other elements) is formed when ash cools after combustion. The larger-size fraction of fly ash within 45 to 75 μm is usually enriched with primary quartz (Williams and van Riessen 2010).

Mullite is formed during coal combustion by decomposed clays (Fig. 2.5b); its crystal structure is formed in the cooling process, rather than directly from minerals in coal (Williams and van Riessen 2010). Mullite typically does not participate in the cementing reaction due to its low reactivity. Since alumina content in high-calcium fly ash is more likely to form C_3A and feldspar, or the alumina content of coal producing high-calcium fly ash is relatively low

originally, high-calcium fly ash contains very little mullite (0.86–1.14 wt%) (Oey et al. 2015), whereas low-calcium fly ash contains about 3–24 wt% mullite (Li 2011, Ramezanianpour 2014, Velandia et al. 2016).

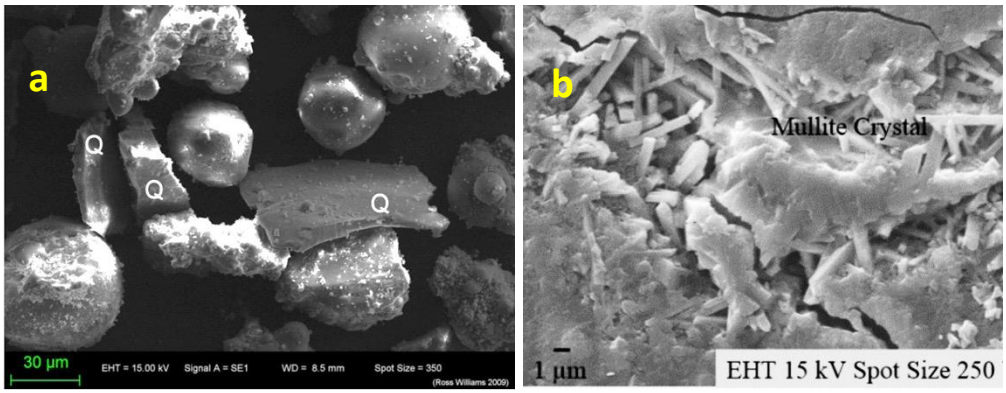

Figure 2.5 SEM micrograph: (a) primary quartz (labelled Q); (b) mullite (Nurgesang et al. 2016; Williams and van Riessen 2010)

Magnetite and hematite contents in all fly ash are relatively close, typically less than 5 wt% (Williams and van Riessen 2010); they are common iron-bearing minerals, governing the magnetic property of magnetospheres (Yang et al. 2014). Anhydrite content (0–10 wt%) is relatively high in high-calcium fly ash, since coal that produces high-calcium ash contains more sulfur (Kutchko and Kim 2006; Tishmack et al. 1999), but it can also be found in other types of fly ash. Anhydrite can react with soluble aluminate to form ettringite, which is beneficial to the self-cementitious property of fly ash (Sheng et al. 2007). The principle sources of alumina in the early stage of fly ash hydration are C_3A and kleinite; the calcium aluminate phase along with free lime determine the heat of fly ash hydration (Wang et al. 2004a).

García-Lodeiro et al. (2013a) reported the development of gels in this hybrid alkaline cement (70% FA+30% OPC) from 28 days to 365 days by using ^{29}Si NMR. At early age, hybrid cement produced a mix of C-S-H/N-A-S-H gels, which was supported by NMR spectra (see Fig. 2.6). The clearly defined peak at -86 ppm indicated a typical $Q^2(0Al)$ structure of C–S–H gel, as

well as typical Q^3(3Al) and Q^4(4Al) structures of N–A–S–H gel. This -86 ppm signal was intensified by NaOH activation (Fig. 2.6c,d), which was attributed to more N–A–S–H gels having Q^3(3Al) and Q^4(4Al) structures (Garcia-Lodeiro et al. 2016). N-A-S-H interacted with Ca over time and developed as follows: N-A-S-H > (N,C)-A-S-H > C-A-S-H, but this development requires sufficient Ca for total conversion. C-S-H would also evolve into C-A-S-H gel, which was considered the most thermodynamically stable form in mixes of aluminosilicate and calcium silicate gels.

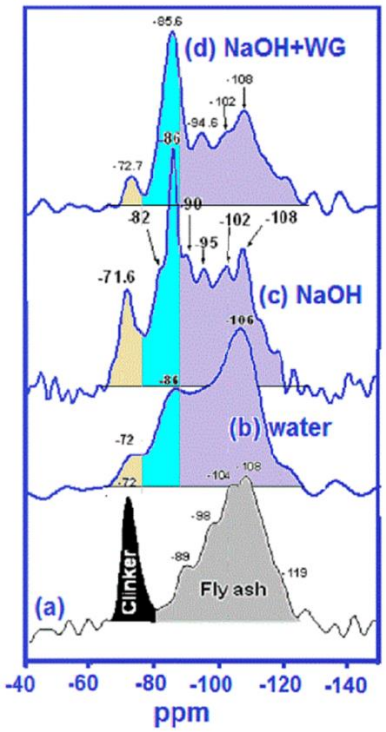

Figure 2.6 29Si NMR spectra: (a) initial mix of 30% OPC + 70% FA; (b) 28-day paste with water; (c) 28-day paste with NaOH; (d) 28-day paste with NaOH + waterglass (WG) (Garcia-Lodeiro et al. 2016)

These conversions did not appear to compromise the strength of the material, as the compressive strength continued to increase between 28 and 365 days (Garcia-Lodeiro et al. 2016). Palomo et al. (2007) showed that an NaOH medium significantly inhibited the hydration of calcium silicate clinker and the formation of portlandite in the first 28 days, which was

evidenced by the highest peak at -72 ppm of unhydrated clinkers in Fig. 2.6c. This observation is explained by Garcia-Lodeiro et al. (2013b): that type of alkaline activators impacted the initial reaction kinetics and proportions of main hydration gels, but did not affect the type of main gels formed.

2.6. Durability of Fly Ash-Based Composites

Although the durability of fly ash-based composites, such as fly ash geopolymer, is superior in many cases (Roy 1999), durability testing of fly ash composites was still required to predict service life and compare with Portland cement concrete. The durability of fly ash-based composites can be evaluated in standards using a performance-based method (Deventer et al. 2015). Durability is often assessed in terms of microstructure, long-term strength development, water absorption and permeability, resistance to sulphate or acid attack, chloride ingress and holding, fire resistance, and efflorescence behavior (Duan et al. 2017, Rashad 2014).

Fernandez-Jimenez et al. (2006) tested the durability of alkali-activated fly ash cement under four conditions: deionized water, sodium sulphate solution, ASTM seawater, and acidic solution. Alkali-activated fly ash (AAFA) mortars were generally more durable than ordinary Portland cement (OPC) mortars regardless of the type of activator used. In the presence of sodium sulphates, a very small amount of degradation product was present in AAFA mortars. Seawater caused a slightly more porous gel microstructure by replacing Na ions with Mg ions. Alkali-activated fly ash mortars showed better resistance to acid attack (HCl) as well. The strength of AAFA mortars declined 23–25%, whereas the strength of OPC mortars declined about 47%. Sugama et al. (2005) tested the resistance of fly ash/slag-based geopolymers to H_2SO_4 with pH value of 1.1. The results indicated that the fly ash/slag mixture with 50/50 proportion had the lowest weight loss. Ismail et al. (2013a) tested the performance of AAFA/slag

geopolymer in 5 wt% $MgSO_4$ and 5 wt% Na_2SO_4 solutions. More damage was caused to the geopolymer by $MgSO_4$ than Na_2SO_4 during the 3-month test, because Mg resulted in decalcification of Ca-rich gel phases, causing binder degradation and the precipitation of gypsum. Na_2SO_4 did not cause substantial degradation of the binder, which was consistent with the findings of another study (Fernandez-Jimenez et al. 2006). Okoye et al. (2017) found that silica fume significantly improved the resistance of fly ash-based geopolymer to the sulphuric acid and chloride solution.

Olivia and Nikraz (2012) used the Taguchi method to optimize the durability and mechanical properties of fly ash geopolymer. Compared with OPC concrete, geopolymer concrete exhibited less expansion and drying shrinkage. Geopolymer concrete also has lower water absorption. Chi and Huang (2013) indicated that the water absorption of AAFA/slag geopolymer decreased as the slag content increased, possibly due to the fact that more active slag produced more gels. The half-cell potential test demonstrated that geopolymer concrete was more susceptible to corrosion than OPC concrete, but its destruction time was 3.86–5.70 times longer than that of OPC concrete. In general, fly ash geopolymer can be used as a more durable alternative to OPC concrete in severe environments.

Curing procedure is another important factor affecting durability performance. Pre-curing at room temperature before heat treatment was considered beneficial to durability (Bakharev 2005). If the curing conditions favor carbonation, the result will be a decrease in pH levels; the fly ash reaction rate, mechanical strength development, and durability will be notably jeopardized. But this carbonation process can be avoided by curing with high humidity (Criado et al. 2010). Freidin (1999) indicated that humid air and water were the most favorable conditions for long-term strength development of fly ash binder. When exposed to air, the

strength development of fly ash binder was divided into three stages: increase of strength in the first month; quick loss of strength during 1 month to 3 or 6 months; stabilization or slowdown of loss of strength after the second stage. This strength loss resulted from the decomposition of unstable ettringite. The duration of the second and third stages depended on the fly ash composition, not on curing conditions (Freidin 1999). But Wang et al. (2004a) noticed that the ettringite formed in the Cement kiln Dust (CKD)-fly ash system remained stable over 100 days, and the elevated curing temperature impaired the crystal ettringite formation at later age.

Zhang et al. (2014) studied the efflorescence behavior of fly ash-based geopolymers. Activators containing soluble silica were found to limit the early-age efflorescence of geopolymers cured at room temperature, but caused the early-age efflorescence of samples cured at 80°C, mainly because samples cured at room temperature developed finer pore size distribution than samples cured at 80°C. Hydrothermal curing and the addition of slag also lead to a lower efflorescence rate (Zhang et al. 2014).

Long-term performance is another important aspect of the durability of fly ash composites. When considering chloride penetration, attention needs to be paid to the long-term performance of fly ash geopolymer with an activator modulus between 1.00 and 1.25, although its durability is comparable to that of OPC concretes (Law et al. 2015). Fly ash can improve the long-term performance of concrete in terms of compressive strength, flexural and tensile strength, creep, drying shrinkage, porosity, capillary absorption, chloride penetration, sulphate attack, and surface scaling. In general, fly ash slightly increased compressive strength, but improved long-term flexural and tensile strength and transport properties of concretes considerably (Gonen and Yazicioglu 2007, Li 2004, Thomas 2007). Class F ash in concrete contributed better compressive strength and resistance to chloride penetration than Class C ash.

The highest long-term compressive strength can be achieved for high-volume fly ash (HVFA) concrete (containing 67% Class F fly ash) at the age of 7 years; HVFA also showed excellent resistance to surface scaling (Naik et al. 2003). Fly ash concrete showed strength development up to 5 years, even with exposure to a marine environment. Fly ash replacement in concrete can reduce the chloride penetration and corrosion of an embedded steel bar (Kwon et al. 2017). Thomas and Bamforth (1999) used predictive models and laboratory test methods to demonstrate that the chloride penetration rate of fly ash concrete during the first 6 months was similar to that of concrete without fly ash. However, after several years of exposure, this rate was greatly reduced in fly ash concrete. When fly ash concrete was exposed to sulphate attack over a long period (600 days), microstructural scale effects could be observed in it, but no significant damage was observed at the macroscopic scale relative to OPC concrete (Chindaprasirt and Chalee 2014, Ortega et al. 2017). Fly ash concrete demonstrated little drying shrinkage: 100 micro strains after 1 year, which is remarkably smaller than that of OPC concrete (500 to 800 micro strains). The creep coefficient of fly ash concrete was found to be 50% of that for OPC concrete (Wallah and Rangan 2006).

All these long-term benefits can be attributed to the pozzolanic reaction of fly ash in concrete, which increases the quantity of C-S-H and C-A-S-H, resulting in cross-linking hydrates at the molecular level and a crack-free dense microstructure, therefore improving long-term durability (Thomas 2007, Wardhono et al. 2017).

2.7. Sustainability of Fly Ash as Construction Material

The use of fly ash with or without alkali activation to replace cement cannot always guarantee the sustainability enhancement of construction. Life cycle assessment (LCA) and cost-benefit analysis (CBA) are often used to evaluate the recycling of fly ash in terms of economic

benefits and environmental influences (Hossain et al. 2017, Wang et al. 2016, Yang et al. 2017). Life cycle assessment is usually carried out according to ISO 14040 standard (ISO 2006). The performance of fly ash as construction material at all levels should be comparable to other commonly used materials, so that the sustainable solution of using fly ash can be accepted in the construction practice.

Seto et al. (2017) established LCA models of concrete containing 10%, 25%, and 50% fly ash as cement replacement. With different LCA allocation scenarios and weighting schemes used, fly ash showed the ability to lower environmental impact by up to 43% (based on Global Warming Potential Index). Marinković et al. (2017) conducted a LCA study on five green concrete mixes with the same compressive strength and workability in two scenarios (Scenario 1: a functional unit of 1 m^3 was adopted, Scenario 2: a functional unit of 1.1 m^3 was adopted for elements made with RCA and FA because they need 5–10% extra height to achieve the equal service life of OPC). Alkali-activated fly ash concrete with natural aggregates showed the least environmental impact despite the high dosage of alkali activators used; conventional concrete with RCA performed worst (Fig. 2.7). However, HVFA concrete with RCA was recommended for in situ applications, as AAFA concrete requires a high curing temperature (80ºC) and is mostly applied to precast concrete structures. Tosun-Felekoğlu et al. (2017), who studied the sustainability of Class C and Class F fly ash in high-tenacity polypropylene engineered cementitious composite applications, found that Class F ash lowered the cost by 45% and reduced CO_2 emissions by 55% compared with conventional polyvinyl alcohol fiber-reinforced engineered cementitious composites.

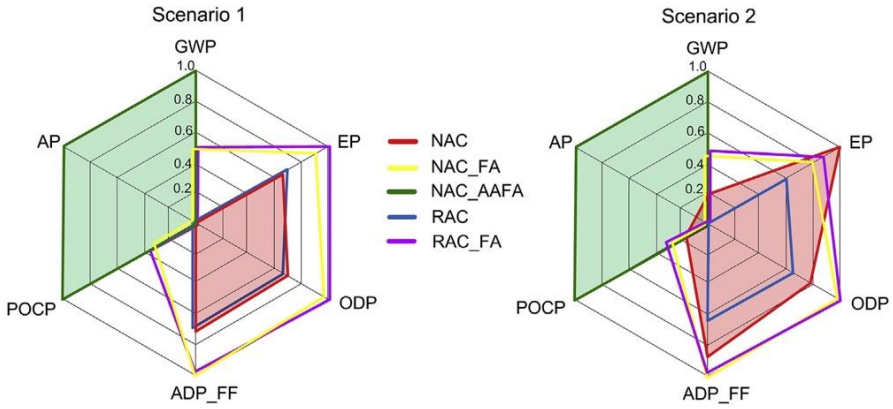

Figure 2.7 Sustainability indicator of different concrete mixes in a "radar" diagram (Marinković et al. 2017)

Huang et al. (2017a) performed CBA on reusing fly ash to calculate the net present value (NPV). The NPV of four scenarios (landfill, ZnO recycling process, recycling as cement, recycling in bricks) showed that recycling as cement offered the highest benefit to economy due to the high sale price of cement. However, when both environmental impact and cost benefit were considered, reuse in the ZnO recycling process was the best option and reuse in a landfill was the least attractive option.

Besides those quantifiable benefits of LCA and CBA, fly ash-based geopolymer shows great potential for greenhouse gas control. Underground injection and storage of CO_2 was proposed to counteract greenhouse gas emission. Fly ash-based geopolymer sealant showed lower permeability of CO_2 (2×10^{-21}–6×10^{-20} m^2) than did OPC sealant (10^{-20}–10^{-11} m^2), effectively preventing CO_2 leakage (Nasvi et al. 2013). Mo et al. (2016) studied fly ash and reactive MgO as cement replacements to uptake CO_2, which typically results in cement degradation, but the MgO-fly ash-OPC system absorbed CO_2 and still resulted in compressive strength gain and dense microstructure due to the formation of (Ca, Mg)CO_3 in the presence of MgO. The role of fly ash in the system was to facilitate carbonation, as it produced a more permeable microstructure. Fly ash-based geopolymers also performed better at adsorbing and

immobilizing toxic metals than OPC. Therefore, fly ash geopolymerization provides an attractive option for the fixation of heavy metals, such as Ba, Cd, Nb, Pb, and Sn, in fly ash and other wastes. These hazardous metals are immobilized in fly ash geopolymer mainly through chemical bonding and physical encapsulation (Zhuang et al. 2016).

Air quality management is another area in which fly ash use shows potential (Balaguera et al. 2018). Research in recent years has shown that the application of fly ash in infrastructure can reduce the emission of CO_2 and other pollutants, as quantified by LCA (Huang et al. 2017b, Poinot et al. 2018, Wang et al. 2017). One study demonstrated that fly ash can be used as an alternative sorbent to carbon to remove NO_x, SO_x, mercury, and other gaseous pollutants from different sources (Ahmaruzzaman and Gupta 2012). More research should be conducted in this area to promote the use of fly ash in the innovative area of sustainability, especially for air quality management.

2.8. Conclusions

Research on fly ash has been extensive since 1900 or earlier. The generation of fly ash will continue to grow for the next decade or more. In-depth knowledge of and extensive experience in the generation, characterization, and application of fly ash have prompted the beneficial use of fly ash as a construction material. Such use can reduce the demand for OPC, divert fly ash from the waste stream, and support cleaner production by reducing emissions, air pollutants, and solid wastes. The following conclusions can be drawn:

1. Fly ash is a fairly complex material in terms of physical, chemical, and mineralogical properties. Combustion temperature, cooling rate, and the composition of fly ash play important roles in determining the physical and cementitious properties of fly ash. High-calcium fly ash is much more complex than low-calcium fly ash in terms of chemical and

mineral composition. Due to its low reactivity, low-calcium fly ash has been widely used as a concrete admixture because it does not dramatically alter the cement hydration chemistry in the short term. Recent years have seen increasing use of high-calcium fly ash based on its growing production; however, the application of high-calcium fly ash in concrete has been hindered because this type of fly ash can change cement hydration significantly and now lacks its reaction model in concrete. Therefore, more research is needed to support the full use of high-calcium fly ash in concrete.

2. Fly ash can be beneficial to the durability and the late-age strength of concrete, as it consumes $Ca(OH)_2$ and induces the formation of secondary hydrates (e.g., C-S-H); it also promotes the formation of strätlingite and C-S-H (I), which are rarely found in the OPC matrix. Hybrid alkaline cement (FA + OPC + Alkali) has become popular, as it eliminates the problem of low early strength and long setting time. Nuclear magnetic resonance study confirms that C-S-H and N-A-S-H formed initially in the FA+OPC system will evolve into C-A-S-H, which is considered the most thermodynamically stable form.
3. Due to the cross-link structure of C-A-S-H gels, the durability of fly ash-based composites is generally superior to OPC concrete (consisting mainly of 1-D or 2-D structures of C-S-H gels) in many respects. Curing procedure is another important factor in the durability performance of fly ash composites.
4. The sustainability of fly ash-based construction materials can be assessed by LCA and CBA. In the literature, AAFA concrete with natural aggregates is reported to have the best overall environmental performance despite the high dosage of alkali activators used; conventional concrete with recycled coarse aggregate (RCA) is reported to have the worst performance. But HVFA concrete with RCA is recommended for in situ applications, as AAFA concrete

requires a high curing temperature. When LCA and CBA are both considered, reusing fly ash in the ZnO recycling process is the best choice.

CHAPTER 3.0 FREEZE/THAW, SALT RESISTANCE, AND STORMWATER INFILTRATION TESTS OF A FLY ASH-BASED PERVIOUS CONCRETE

3.1 Introduction

Pervious concrete is a special type of concrete; its high porosity allows water from precipitation and other sources to pass through directly into the base/subbase and underlying soil. The infiltration effect provided by pervious concrete pavements can recharge groundwater and reduce the amount of total suspended solids, total phosphorus, total nitrogen, and metals in groundwater (Schaefer et al. 2006a). A typical pervious concrete mix design contains Portland cement, the environmental footprint of which raises concerns related to high-energy consumption, release of air pollutants (NO_x and SO_2), and greenhouse gases (CO_2). In this study, to make pervious concrete environmentally friendly and sustainable, fly ash, a by-product of coal-fired power plants, has been chosen to fully replace Portland cement in pervious concrete. Fly ash has been used as partial cement replacement in concrete for years (Roskos 2011, Harwalkar and Awanti 2014, Palomo et al. 1999, Schneider et al. 2011).

Significant quantities of fly ash are generated every year. In 2013, the United States produced 115 million tons of coal ash. Only 45% was used beneficially; nearly 64 million tons were disposed of (Minkara 2015). Based on analytical CaO content, fly ash can be divided into high-calcium fly ash (CaO content > 10%) and low-calcium fly ash (CaO content < 10%) (Fan et al. 2015). Recent years have seen increasing use of younger lignite or sub-bituminous coal at power plants, which has led to increasing availability of high-calcium fly ash (Guo et al. 2010).

Berry et al. (2011) have demonstrated that it is possible to use high-calcium fly ash as the sole cementitious binder in making concrete of moderate strength.

One notable barrier to the implementation of pervious concrete pavement is its lack of durability in cold climates (Shi et al. 2017, Xu and Shi 2018a, Xu et al. 2011, Xu et al. 2017b, Yang et al. 2011). Specifically, the use of chemical deicers in cold regions tends to exacerbate the susceptibility of concrete infrastructure to freeze/thaw (F/T) cycles (Anderson and Dewoolkar 2015, Shi et al. 2009, Valenza and Scherer 2007). Relative to impervious concrete, pervious concrete is more prone to the ingress of water and deicer solution and is thus more vulnerable to premature failure due to salt scaling damage. Previous studies (Amde and Rogge 2013, Yang et al. 2006) found that pervious concrete has weak resistance to F/T cycles.

In this work, the F/T resistance and the ambient-temperature salt resistance of pervious concrete specimens were investigated separately, to isolate the physical and chemical phenomena underlying deterioration during the "salt scaling" test, which combined the effects of F/T cycling and deicer attack. Sustainable pervious concrete with fly ash as the sole binder was developed with alkali activation at room temperature. Graphene oxide (GO) was used to facilitate the polymerization of reaction products from alkali activation. Studies by Lv et al. (2014), Gong et al. (2015, and Ranjbar et al. (2015) indicated that GO can improve the overall performance of cement mix by regulating cement hydration, providing a crack branching and bridging mechanism, and acting as nanofillers. Therefore, GO has significant potential for application in fly ash-based pervious concrete of high strength and durability.

The following sections detail the material preparation, fabrication, F/T testing and wet-dry (with salt solutions) testing of pervious concrete. The microstructural characterization of

GO-modified fly ash concrete was also carried out through X-ray powder diffraction (XRD) analysis and nuclear magnetic resonance (NMR) spectroscopy.

3.2 Research Significance

The physical and chemical phenomena underlying the deterioration of pervious concrete in cold-climate service conditions were investigated. The NMR study revealed the hydrate structure of GO-modified fly ash and cement pervious concrete, shedding light on the fundamental difference in performance between fly ash and cement hydrates at the molecular level.

3.3 Experimental Study

3.3.1 Material

The *high-calcium* fly ash used in this study was obtained from a power plant in Oregon, a state in the U.S. Fly ash compositions were examined by X-ray fluorescence (XRF) analysis (see Table 3.1). Loss on ignition was acquired through thermogravimetric analysis.

Table 3.1 Physical and chemical properties of the fly ash and glass powder (% wt.)

	Glass powder	**Fly ash**
Specific gravity	2.6	2.5
Bulk density (lb/ft^3) [kg/m^3]	43 [689]	54 [860]
d98 top size (μm)	40	--
D50 median size (μm)	8–9	--
SiO_2 (wt. %)	50–55%	23.5%
CaO (wt. %)	20–25%	23.2%
Al_2O_3 (wt. %)	14–20%	13.8%
Fe_2O_3 (wt. %)	<1%	4.8%
MgO (wt. %)	<2%	4.2%
Na_2O+K_2O (wt. %)	8–14%	6.7%
Loss on ignition (wt. %)	<0.5%	≈ 0.8%

The amount of chemical activators designed to facilitate dissolution of fly ash and polymerization of hydration products is as follows:

- Water glass, i.e., sodium silicate ($Na_2SiO_3.9H_2O$): 7% by weight of fly ash
- Sodium sulphate ($Na_2SO_4.10H_2O$): 1% by weight of fly ash
- Quicklime (CaO): 5% by weight of fly ash
- Calcium chloride ($CaCl_2.2H_2O$): 0.5% by weight of fly ash

The GO used in this study was produced by using a modified Hummer's method, which mainly involves chemical oxidation of the graphite (Li et al. 2008). The as-produced GO was pasty; it was diluted with deionized water first and then sonicated for 45 minutes using a Branson digital sonifier (S-450D, 400 W, 50% amplitude) to produce stable GO suspension (Fig. 3.1). The major elements of GO were C = 71 wt.% and O = 26 wt.%.

Figure 3.1 Ultrasonification of GO suspension

One type of single-sized coarse aggregate, crushed limestone 3/8 inch in size, was used. One commercially available glass powder, recycled from industrial feedstocks, was used as

micro-filler in the pervious concrete mix design to improve workability and sustainability. The properties of this glass powder are listed in Table 3.1. A Type I/II cement was used in the mix design of control groups.

3.3.2 Mix Proportions

Four groups of pervious concrete were designed to investigate the performance of fly ash-based pervious concrete under F/T and wet-dry cycles. The proportions of the four mixes are shown in Table 3.2. Triethanolamine (TEA) was used to improve the early-age strength of the pervious concrete. An air-entraining (AE) agent, MB-AE 90, and a high-range water reducer (HRWR), MasterGlenium 7920, were used to improve the workability and F/T resistance of the pervious concrete.

Table 3.2 Pervious concrete material proportions

Mix Design	**Agg. Size (mm) [inch]**	**Agg. (kg/m^3) [lb/ft^3]**	**Cement (kg/m^3) [lb/ft^3]**	**Fly ash (kg/m^3) [lb/ft^3]**	**Water (kg/m^3) [lb/ft^3]**	**GO (g/100kg binder)***	**TEA (ml/100kg binder)***	**HRWR (ml/100kg binder)***
Cement	9.5 [3/8]	1425 [89]	320 [20]	--	80 [5]	--	40	300
Cement + GO	9.5 [3/8]	1425 [89]	320 [20]	--	80 [5]	20	40	300
Fly ash	9.5 [3/8]	1425 [89]	--	320 [20]	80 [5]	--	40	1000
Fly ash + GO	9.5 [3/8]	1425 [89]	--	320 [20]	80 [5]	20	40	1000

* 2% (by weight of fly ash) glass powder used
* Air entraining agent dosage = 30ml/100kg binder for all mix designs
* 1 fl oz/cwt = 65.2 mL/100 kg, 1 oz/cwt = 62.5 g/100kg
* Fly ash weight includes the designed amount of chemical activators

Prismatic test specimens (3 × 4 × 16 in. [76 × 102 × 406 mm]) were used according to ASTM C666 (ASTM C666 / C666M-15 2015). The concrete was mixed and cast in steel molds in accordance with ASTM C192 (ASTM C192/C192M 2016). The specimens were demolded

after 24 hours, and cured for 14 days before the testing. Six fly ash-based specimens were cured for 28 days to test the effects of longer curing time.

3.4 Test Procedures

3.4.1 Freeze/thaw test

The F/T tests were carried out according to ASTM C666 Procedure A (ASTM C666 / C666M-15 2015). By design, this test protocol investigates the resistance of pervious concrete to F/T damage in an accelerated manner, as pervious concrete shows weak resistance to F/T cycles when tested under fully saturated (i.e., undrained) conditions (Amde and Rogge 2013, Yang et al. 2006) (Fig. 3.2), which is usually not representative of properly designed and constructed pervious concrete pavements in the field service environment. Freeze/thaw damage was also evaluated based on changes in the dynamic modulus of elasticity (E), in accordance with ASTM C215 (ASTM C215-14 2014). Mass loss of the samples was measured, with 15% loss considered failure (Schaefer et al. 2006b). $P_{f/t}$ is referred to as the relative dynamic E for F/T testing.

Figure 3.2 Pervious concrete specimens in the freeze/thaw chamber (undrained)

3.4.2 Wetting and drying in solutions of NaCl

For the wet/dry exposure test, we adopted procedures used in a previous study (Darwin et al. 2008), where pervious concrete specimens were exposed to weekly cycles of wetting and drying in a 3 wt% solution of NaCl. Three specimens were used for each of the mix designs in Table 3.2. The specimens were submerged in the NaCl solution for 4 days at a temperature of 72 ± 4°F (22 ± 2°C). The specimens were then removed from the solution and dried in air at the same temperature for 3 days. The deicer solutions were replaced every 5 weeks.

Similar to the F/T test in ASTM C666 (ASTM C666 / C666M-15 2015), the effects of wet-dry cycles were evaluated based on changes in the dynamic modulus of elasticity in accordance with ASTM C215 (ASTM C215-14 2014). The fundamental transverse resonance frequency of each specimen was measured before the test and every 2 weeks thereafter; the dynamic *E* was calculated based on the mass, dimensions, and fundamental frequency of the specimen according to ASTM C215 (ASTM C215-14 2014). The ratio ($P_{w/d}$) of dynamic *E* at the given number of cycles to the initial dynamic *E* is referred to as the relative dynamic *E* for wet/dry testing.

3.4.3 NMR and XRD tests

^{29}Si and ^{27}Al Magic Angle Spinning (MAS) NMR spectroscopy was performed on the freshly ground paste samples at 56 days, using a Bruker solid-state NMR instrument with a magnetic field strength of 7.05 T, packed in 4 mm ZrO_4 rotors and spun at 5 or 12 kHz at ambient temperature. ^{29}Si spectra (operating frequency of 59.5 MHz) were acquired between 1000 and 7500 scans using a pulse recycle delay of 15 s, a pulse width of 1.2 μs, and an acquisition time of 80 ms. ^{29}Si chemical shifts were referenced to tetramethylsilane (TMS) at 0

ppm. The samples were spun for no longer than 60 min to avoid dehydration of the sample and loss in the intensity of peaks (Richardson et al. 2016). The NMR test results are presented in Chapter 4. Powder XRD patterns were collected for the paste samples after failure in the NaCl solutions, using an X-ray diffractometer with an incident beam of Cu-Kα radiation (λ = 1.5418 Å) for a 2θ scanning range of 5°–70°.

3.5 Experimental Results and Discussion

3.5.1 Specimens in the freeze/thaw test

To evaluate the F/T resistance of pervious concrete, the change of fundamental transverse resonance frequency over the F/T cycles was measured and recorded (see Table 3.3). The variation of relative dynamic E (calculated based on Table 3.3 as $P_{f/t}$) with respect to the number of F/T cycles is presented in Fig. 3.3, which provides a good indication of the deterioration of pervious concrete over the entire duration of F/T cycles. Figure 3.3 includes the resistance to F/T cycles of five groups: Portland cement pervious concrete cured for 14 days, GO-modified cement pervious concrete cured for 14 days, fly ash pervious concrete cured for 14 days, fly ash pervious concrete cured for 28 days, and GO-modified fly ash pervious concrete cured for 28 days. The specimens after failure are shown in Fig. 3.4.

Table 3.3 Average transverse resonance frequency (Hz) and coefficients of variation for specimens in freeze/thaw cycles

	Cement-14d		**Cement+GO-14d**		**Fly Ash-28d**		**Fly Ash+GO-28d**	
Cycles	**Average**	**COV**	**Average**	**COV**	**Average**	**COV**	**Average**	**COV**
0	1832	0.015	1806	0.032	1452	0.039	1733	0.035
6	1823	0.016	1791	0.031	1379	0.044	1701	0.027
12	1800	0.028	1772	0.027	1349	0.013	1691	0.030
36	1789	0.005	1672	0.015	1283	0.019	1683	0.032

	Cement-14d		Cement+GO-14d		Fly Ash-28d		Fly Ash+GO-28d	
Cycles	**Average**	**COV**	**Average**	**COV**	**Average**	**COV**	**Average**	**COV**
60	1737	0.047	1662	0.066	24	0.062	1619	0.029
96	1571	0.057	1586	0.081	failed	--	1570	0.039
144	30	0.057	1488	0.084	--	--	30	0.023
162	failed	--	30	0.039	--	--	failed	--

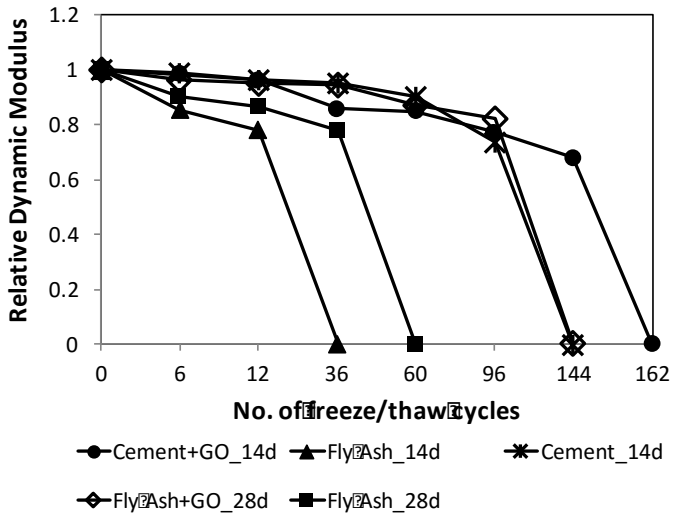

Figure 3.3 Relative dynamic modulus of elasticity (Pf/t) versus number of freeze/thaw cycles

a **b** **c** **d**

Figure 3.4 Failed specimens after the freeze/thaw test, (a) Fly Ash_28d group; (b) Fly Ash+GO_28d group; (c) Cement+GO_14d group; (b) Cement_14d group

As shown in Fig. 3.3, the fly ash pervious concrete specimens cured for 14 days before testing experienced total failure at 36 cycles, whereas specimens cured for 28 days before testing experienced total failure at 60 cycles, indicating fly ash hydration was a slow process and fly ash pervious concrete presented better resistance to the F/T test at later ages. After adding GO, the fly ash pervious concrete (cured for 28 d) experienced a total failure at 144 cycles, showing equal durability characteristics compared with those of conventional cement pervious concrete (cured for 14 d), which also experienced total failure at 144 cycles. After adding GO, the total failure of cement pervious concrete was delayed from 144 cycles to 162 cycles.

Overall, GO showed the ability to improve resistance to F/T cycles for both cement and fly ash pervious concretes. Due to the slow hydration of fly ash (chemically activated hydration in fly ash versus spontaneous hydration in cement), the F/T resistance of GO-modified fly ash pervious concrete cured for 28 days can only be comparable to the cement pervious concrete cured for 14 days.

3.5.2 Specimens in the wet/dry test with NaCl solutions

To evaluate the negative impact of NaCl on pervious concrete in wet/dry cycles, the change of fundamental transverse resonance frequency was measured and recorded (see Table 3.4). The variation of relative dynamic E (calculated based on Table 3.4 as $P_{w/d}$) with respect to the number of wet/dry cycles is presented in Fig. 3.5, which provides a good indication of the deterioration of pervious concrete in NaCl solution. Figure 3.5 includes the resistance to wet/dry cycles of four groups: cement pervious concrete cured for 14 days, GO-modified cement pervious concrete cured for 14 days, fly ash pervious concrete cured for 14 days, and GO-modified fly ash pervious concrete cured for 14 days.

Table 3.4 Average transverse resonance frequency (Hz) and coefficients of variation for specimens in wet/dry cycles

	Cement-14d		Cement+GO-14d		Fly Ash-14d		Fly Ash+GO-14d	
Cycles	**Average**	**COV**	**Average**	**COV**	**Average**	**COV**	**Average**	**COV**
0	1816	0.046	1720	0.051	1398	0.163	1547	0.111
1	1769	0.039	1755	0.057	1292	0.190	1456	0.110
2	1841	0.041	1757	0.059	1331	0.165	1531	0.082
4	1798	0.034	1741	0.047	1411	0.166	1584	0.084
6	1749	0.039	1675	0.065	1525	0.140	1726	0.040

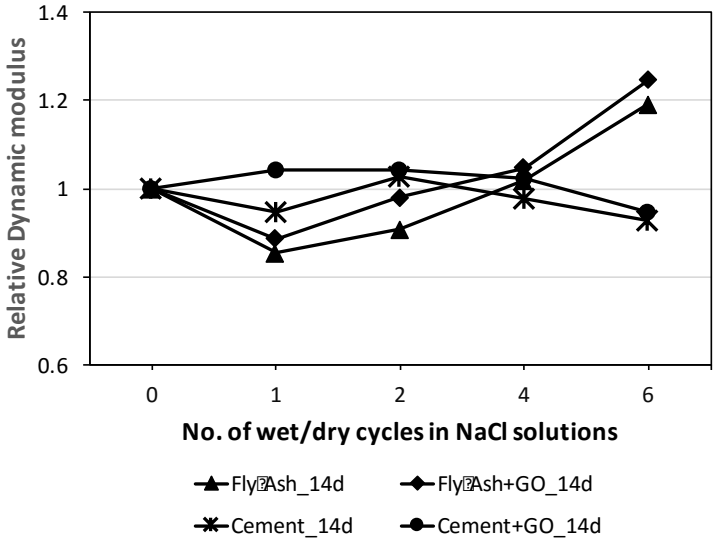

Figure 3.5 Relative dynamic modulus of elasticity (Pw/d) versus number of wet/dry cycles in NaCl solutions

As shown in Fig. 3.5, the $P_{w/d}$ of cement pervious concrete generally decreased as the cycle increased. The $P_{w/d}$ of fly ash specimens decreased after the first cycle; however, it showed an increasing trend afterwards. After adding GO, the resistance to wet/dry cycles in NaCl solution was improved for both cement and fly ash pervious concretes. Previous studies (Lee et al. 2000, "Thomas Telford Bookshop – Civil Engineering Publications" n.d.) indicate that salts can affect the chemistry of cement paste, as chloride solutions cause the formation of calcium

chloride hydrate and calcium oxychloride. The decrease of $P_{w/d}$ in cement pervious concrete can be related to the formation of these phases. The increase of $P_{w/d}$ in fly ash pervious concrete can be attributed to both the slow strength gain and the different chemistry of fly ash pastes, which were examined by XRD and NMR methods later.

Overall, GO showed the ability to improve resistance to NaCl attack for both cement and fly ash pervious concretes. Fly ash pervious concretes exhibited better resistance to NaCl than their cement counterparts. While the F/T test caused rapid physical damage to pervious concrete, the salt attack caused slow deterioration of the specimens.

3.5.3 XRD analysis

The pastes after wet-dry cycles in salt solutions were further examined by the XRD analysis. Figure 3.6 shows the XRD patterns of the different samples. In the pastes of ordinary fly ash and cement pervious concrete, the XRD patterns indicate the presence of calcite (at 23.1°, 29.4°, 36.1°, 39.6°, 43.2°, 47.6°, and 48.5°) as a predominant crystal phase because the salt attack caused by NaCl along with carbonation resulted in paste decalcification (Valenza and Scherer 2007). A wide shoulder-band was observed between 25° and 35° in all samples, indicating the presence of C-S-H gels around 30° (Jeon et al. 2015). The pastes of Cement+GO and Fly Ash+GO groups showed a decrease in calcite peaks and an increase in portlandite peaks (at 18.2°, 28.9°, 34.3°, 47.4°, 50.1°, and 54.5°), indicating that GO improved the resistance of concrete to carbonation in salt solutions, which is likely related to the formation of GO-improved hydrates. The absence of gypsum peak (at 45.5°) in the Fly Ash+GO and Cement+GO pastes is another evidence of GO-improved resistance to carbonation, as the carbonation of ettringite forms calcium carbonate and gypsum. Hatrurite (a mineral form of alite) at 32.4°, 41.5°, and

52.0° and larnite (a mineral form of belite) at 32.7° were overserved as non-hydrated mineral parts of fly ash and cement (Schmidt et al. 2012). Quartz was also detected in the cement pastes.

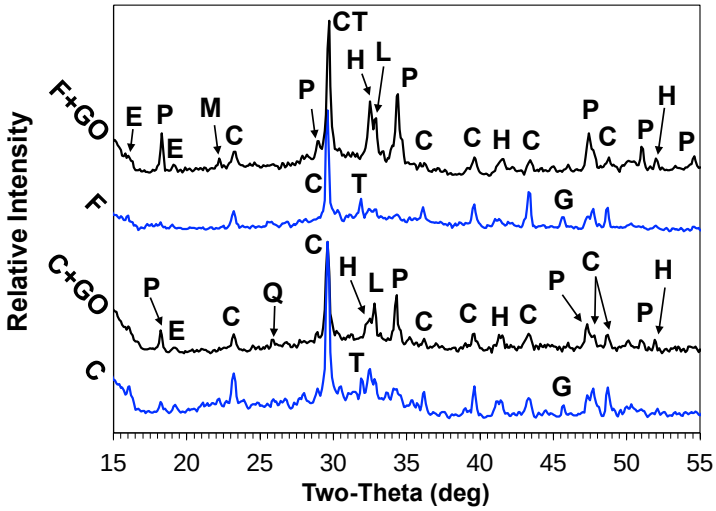

Figure 3.6 XRD patterns of pervious concrete pastes after the deicer salt scaling test. C: calcite, CT: clinotobermorite, E: ettringite, G: gypsum, H: hatrurite, L: larnite, M: margarite, P: portlandite, Q: quartz, T: tobermorite.

Peaks from pozzolanic products, margarite ($CaAl_4Si_2O_{11}.H_2O$) at 22.2° and clinotobermorite ($Ca_5Si_6O_{17}.5H_2O$) at 29.7°, were observed in the Fly Ash+GO group only. Peak at 31.8° is from the semi-crystalline C–S–H (I) (Richardson 2014), which is essentially a tobermorite, and its peak stands out in the patterns of Fly Ash and Cement pastes, suggesting it resists salt attack better. Fly Ash+GO concrete showed the best performance in the wet/dry cycles, as GO facilitated the formation of these two pozzolanic hydrates (margarite and clinotobermorite) to provide better resistance (Lothenbach et al. 2011) to salt attack. Ismail et al. (2013b) stated that a Al-substituted calcium silicate hydrate (C-A-S-H) (analogy to margarite) contributes to higher durability under chloride exposure. Merlino et al. (1999) indicated that clinotobermorite, a typical CSH mineral, has a condensed molecular structure, which contributes to better salt resistance.

Fly ash and cement pervious concrete specimens were exposed to F/T cycles and wet/dry cycles in NaCl solutions. The effects of exposure were evaluated based on changes in the dynamic modulus of elasticity. X-ray diffraction (XRD) and nuclear magnetic resonance (NMR) were employed to explain the difference in specimen performance in terms of minerology and chemical structure. The following conclusions can be drawn.

1. Due to the slow hydration of fly ash, the F/T resistance of GO-modified fly ash pervious concrete cured for 28 days was comparable to the cement pervious concrete cured for 14 days. Graphene oxide improved resistance to F/T cycles for both cement and fly ash pervious concretes.
2. Fly ash pervious concrete showed better resistance to NaCl than cement concrete. Compared with the F/T test, which caused rapid physical damage to pervious concrete, the salt attack caused specimens to deteriorate slowly. Graphene oxide also improved the resistance of cement and fly ash pervious concretes to NaCl attack.
3. Graphene oxide promoted the formation of semi-crystalline C–S–H (I) and C-A-S-H gels in fly ash hydrates, which provided better resistance to the salt attack.

3.5.4 Stormwater infiltration tests

The ability of GO-modified fly ash pervious concrete to treat deicer-laden stormwater was evaluated. Portland cement pervious concrete was used as the control to compare with GO-modified fly ash pervious concrete. Apart from the commonly used deicers (NaCl and $CaCl_2$) in cold regions, chemicals were chosen to represent other possible pollutants in stormwater: copper, zinc, sulphate, ammonia, nitrate, and total phosphate. Although previous studies showed that cement pervious concrete effectively reduced pollutant concentrations in stormwater through a

combination of mechanical and biological methods that make pervious concrete a best-management practice for stormwater control, such an ability in GO-modified fly ash pervious concrete remained unknown in Phase I.

The actual stormwater was collected on the curbside (Fig. 3.7). All the determinations of contamination in stormwater were done with inductively coupled plasma quadrupole mass spectrometry (ICP-Q-MS). This type of spectrometry is a relatively new method for determining multi-element analysis, and it is ideal for water. The collected stormwater was poured on top of the pervious concrete specimens (4" × 4" × 10" bars). Two groups of specimens were tested: FA+GO and Cement (see Table 3.2). Infiltrated stormwater was then collected at the bottom of the pervious concrete specimens (Fig. 3.8). Concentrations of different contaminants were determined before and after this test (each test used six stormwater samples). The collected runoff samples were slowly poured on top of the pervious concrete to ensure that no water was leaking out of the sides.

Figure 3.7 Stormwater collected at curb side

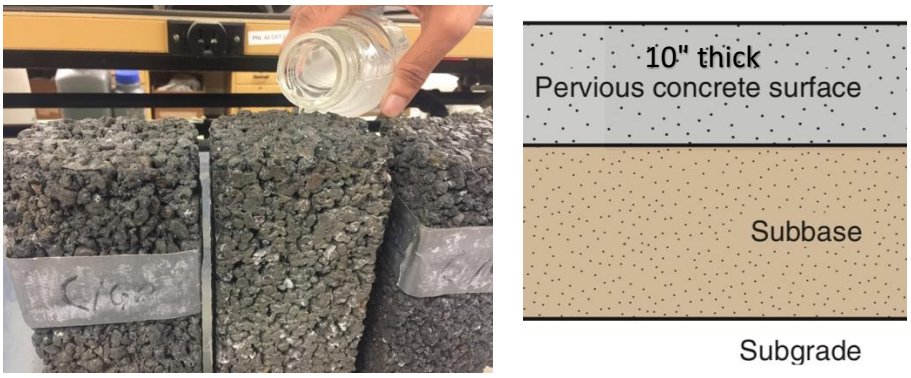

(a) (b)

Figure 3.8 Actual stormwater infiltration test (a) and simulated case (b)

Table 3.5 presents the contaminant concentrations in the collected stormwater runoff (a total of six samples were tested). Table 3.6 presents the contaminant concentrations after testing. Test results indicate that the concentrations of possible pollutants in stormwater—copper, zinc, sulphate, chloride, lead, total nitrate, and total phosphate—showed different degrees of reduction (ranging from 2% to 35%) after running through the pervious concrete. The ability of pervious concrete to remove pollutant concentrations was evaluated per the reduction factors for different pollutants. The fly ash pervious concrete showed better reduction factors than the cement pervious concrete, on sulphate, lead, chloride, total phosphate, and nitrate. Especially for chloride content, fly ash pervious concrete introduced 35% reduction, much higher than the 19% reduction of cement pervious concrete. Thus, fly ash pervious concrete shows great potential as an effective means of addressing the deicer-laden stormwater issue in cold regions and supports environmental stewardship. This, of course, is based on the assumption that fly ash pervious concrete can be further engineered to maintain its integrity after exposure to deicer-laden stormwater.

Table 3.5 ICP-MS results of contaminants in stormwater before testing

Constituent	Stormwater Runoff (mg/l)	
	Range	Average
Copper	250-325	100
Zinc	0.02-3.40	1.02
Sulphate	2.20-22.40	5.42
Lead	0.02-1.90	0.24
Chloride	3.20-7.40	5.20
Total Phosphate	0.04-6.20	0.72
Total Nitrate	0.7-22.20	5.30

Table 3.6 ICP-MS results of contaminants in stormwater after testing

Constituent	Stormwater Runoff After Treatment (mg/l)				Residual Factor	
	FA+GO pervious concrete		Cement pervious concrete		FA+GO	Cement
	Range	Average	Range	Average		
Copper	191–301	87	188–297	85	0.87	0.85
Zinc	0.18–3.20	1.00	0.15–2.98	0.98	0.98	0.96
Sulphate	1.80–18.40	4.33	2.02–20.11	4.89	0.80	0.90
Lead	0.01–1.67	0.20	0.02–1.88	0.22	0.91	0.92
Chloride	2.10–6.30	3.40	2.45–6.98	4.23	0.65	0.81
Total Phosphate	0.02–5.20	0.62	0.03–5.87	0.66	0.86	0.92
Total Nitrate	0.65–19.70	5.10	0.82–20.13	5.23	0.96	0.98

CHAPTER 4.0 CHARACTERIZATION OF FLY ASH BINDER

4.1 Introduction

Research carried out on the function of graphene oxide (GO) in conventional cementitious binders shows that this new nanomaterial has significant potential to become an outstanding admixture to binder materials (Gong et al. 2015, Lv et al. 2014, Saafi et al. 2015, Ranjbar et al. 2015). However, little research has been conducted to investigate the performance and compatibility of GO in a fly ash geopolymer. Alkali-activated fly ash geopolymer is distinguished from cement by its higher initial alkalinity and lower availability of Ca^{2+} ions (Garcia-Lodeiro et al. 2011). Also, the hydration products tend to form Ca(Na, K)-A-S-H (aluminosilicate hydrate) gels instead of C-(A)-S-H (aluminate-substituted calcium silicate hydrate) gels (Shi et al. 2017, Xu et al. 2018, Xu and Shi 2017a,b, 2018b,c). As such, the prediction of GO's performance in alkali-activated fly ash binder made based on ordinary cement binder may be inappropriate.

Research is needed to obtain an enhanced understanding of the reaction mechanism of GO in the fly ash hydration system and to improve the solidification of fly ash as a geopolymer material. In this chapter, the possible role of GO in a chemically activated fly ash binder is examined, based on experimental results. The authors hypothesized that GO dispersed in chemically activated fly ash binder can be employed as growth points and templates to facilitate fly ash hydration and modify the structure of hydration products at the molecular level, which in turn improves the mechanical performance of fly ash geopolymer. The following sections detail the investigation of GO's function through the fabrication, testing, and microstructural

characterization of a chemically activated fly ash binder used in pervious concrete (without the use of strong alkali or heat).

4.2 Experimental Raman Spectroscopy

The main role of activators is to dissolve the aluminosilicate fly ash to provide hydration precursors. The dissolution of solid aluminosilicate materials in the alkaline aqueous solution was categorized into two general types (Dimas et al. 2009): congruent dissolution, the dissolution of waste aluminosilicate materials with complex composition, such as fly ash, which produces aqueous monomeric species of Si and Al; and incongruent dissolution, the dissolution of industrial minerals such as kaolinite, which produces oligomeric molecular units. These aqueous monomeric species of silicates and aluminates have been well studied (Šefčík and McCormick 1997, Swaddle 2001, Swaddle et al. 1994). It was found that tetrahedral $Al(OH)_4^-$ was the only important Al species in solutions at pH = 7 to 13, which is observed as a 620 cm^{-1} band in Fig. 4.1. The dissolved silica is observed primarily as $Si(OH)_4$ (symmetric stretching at 730 cm^{-1}), $SiO(OH)_3^-$(Si-O stretching at 1020 cm^{-1}) and $SiO_2(OH)_2^{2-}$(Si-O stretching near 928 cm^{-1}) in Fig. 4.1. As the pH value decreased (from 1 hr to 24 hr), the band of $SiO(OH)_3^-$anions disappeared. Two regions, -Si-O-Si- vibrational modes (475–650 cm^{-1}) in oligomers and $Si\text{-}O^-$ stretching modes in all deprotonated species (850–1125 cm^{-1}) (Hunt et al. 2011), are marked in Fig. 4.1.

The AFt (Al_2O_3–Fe_2O_3-tri) phase (with peaks nearing 986 cm^{-1}) and AFm (Al_2O_3–Fe_2O_3-mono) phase (with peaks nearing 975 cm^{-1}) were detected in the Raman spectra. For GO-modified fly ash pastes, the AFm phase observed at 6 hr was shifted to AFt at 24 hr in Fig. 4.1b, whereas the AFt phase observed at 6 hr was converted to AFm at 24 hr in the ordinary fly ash paste. Garg et al. (Garg et al. 2013) also observed a sudden shift of position of these peaks during

12–20 hr, which may result from either recrystallization of ettringite or the initial formation of AFm. Garg et al. (2013) explained that the oscillation between AFt and AFm phases, as seen by the dual peaks at early ages, was related to the high amount of iron present in the fly ash.

Table 4.1 provides a summary of peak assignments and references used for this Raman study. It is important to note that the intensity of Q^3 Si and quartz bands was increased after adding GO, indicating GO could facilitate the formation of these phases at 24 hr. As hydration continued, a broad shift (ranging from 700 to 800 cm^{-1}) of a tricalcium aluminate phase disappeared fast.

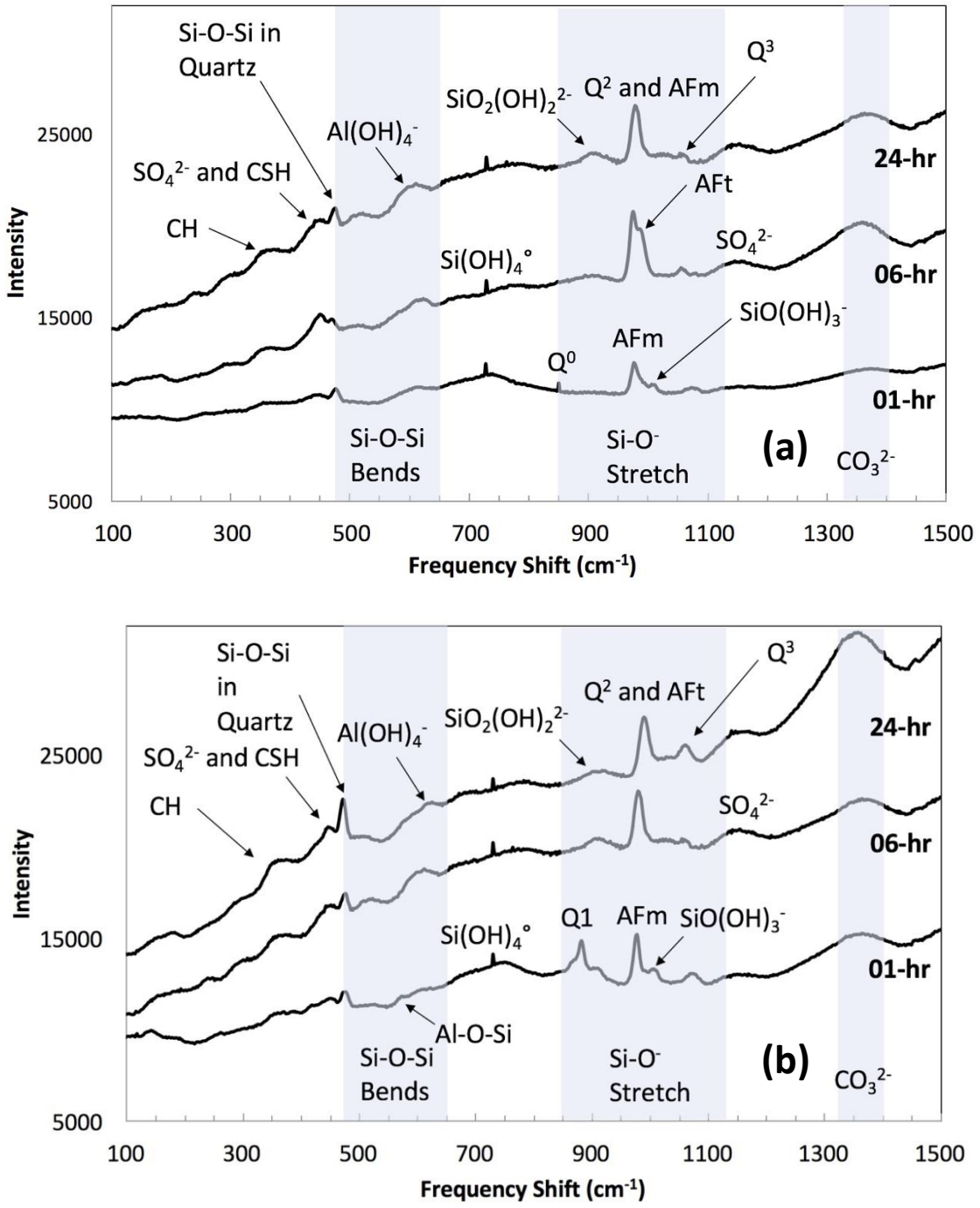

Figure 4.1 Raman spectra of pastes taken at ambient condition: (a) fly ash pastes; (b) GO-modified fly ash pastes

Table 4.1 Summary of Raman spectra investigation

Unit	Frequency Shift	Ref.	GO's influence on intensity at 24 h
Al-O-Si	~574	Gout et al. 2000	↓
$Al(OH)_4^-$	620	Gout et al. 2000	↔
AFm	~975	Garg et al. 2013; Liu et al. 2015	↓
AFt	986	Liu et al. 2015	↑
CH	356–359	Liu et al. 2015	↔
C-S-H	450	Liu et al. 2015	↔
Q^0 Si	~850	Garg et al. 2013	↔
Q^1 Si	870–900	Garg et al. 2013	↔
Q^2 Si	950–1010	Garg et al. 2013	↔
Q^3 Si	1050–1100	Garg et al. 2013	↑
Si-O-Si in Quartz	475	Potgieter-Vermaak et al. 2006	↑
$Si(OH)_4^0$	730	Gout et al. 2000; Hunt et al. 2011	↔
$SiO(OH)_3^-$	1020	Gout et al. 2000; Hunt et al. 2011	↔
$SiO_2(OH)_2^{2-}$	927–928	Dutta and Shieh 1985; Gout et al. 2000	↔
SO_4^{2-}	450 (v_2) & 1140 (v_3)	Kloprogge et al. 2002	↔
C_3A	700–800	Potgieter-Vermaak et al. 2006	↔

4.3 Microscopic Investigation

The BSE (backscattered electron) and SEI (secondary electron image) micrographs of a representative area in two different fly ash mortars are shown in Fig. 4.2. While SEI micrographs provide only morphological information, BSE images additionally provide compositional information by discriminating heavy versus light atoms. That is, the heavier elements typically appear brighter than the lighter elements in BSE images (Bodor et al. 2016). By using chemical activators at room temperature, fly ash spheres (shown in Fig. 4.2a) clearly exhibited different levels of dissolution: some spheres partially dissolved, some collapsed, whereas some were only at the onset of dissolution. The dissolution of fly ash provided the precursors for various hydration products. By comparing the morphology of GO-modified fly ash hydrates (Fig. 4.2b)

with that of regular fly ash hydrates (Fig. 4.2a), no obvious conclusions could be drawn regarding the function of GO in the fly ash hydration system. Therefore, in-depth studies (elemental mapping analysis and NMR) were conducted to investigate GO's role in this fly ash binder.

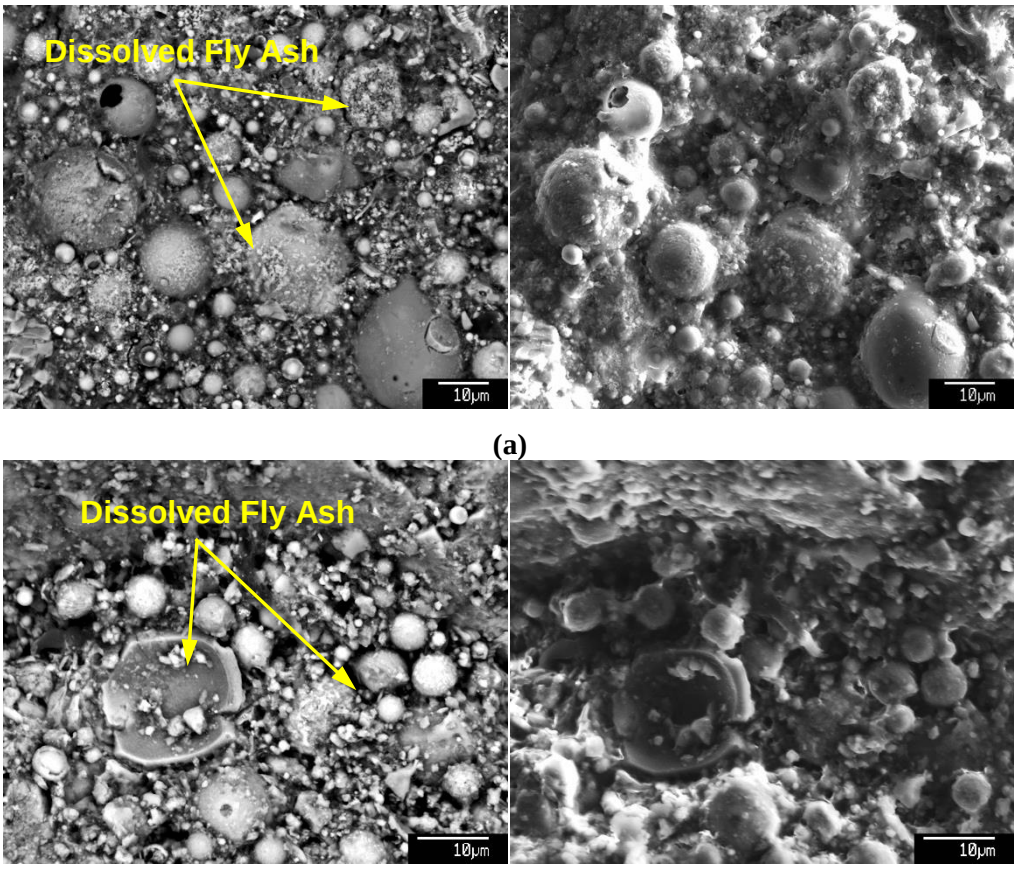

Figure 4.2 BSE (left) and SEI (right) micrographs at 28-d: (a) ordinary fly ash mortar; (b) GO-modified fly ash mortar

4.4. Elemental Mapping

Mapping images of four elements (Al, Ca, Si, and S) were generated for both the ordinary fly ash mortar and the GO-modified fly ash mortar to investigate the influence of GO from the perspective of elemental distribution at the microscopic level (Fig. 4.3, Fig. 4.4).

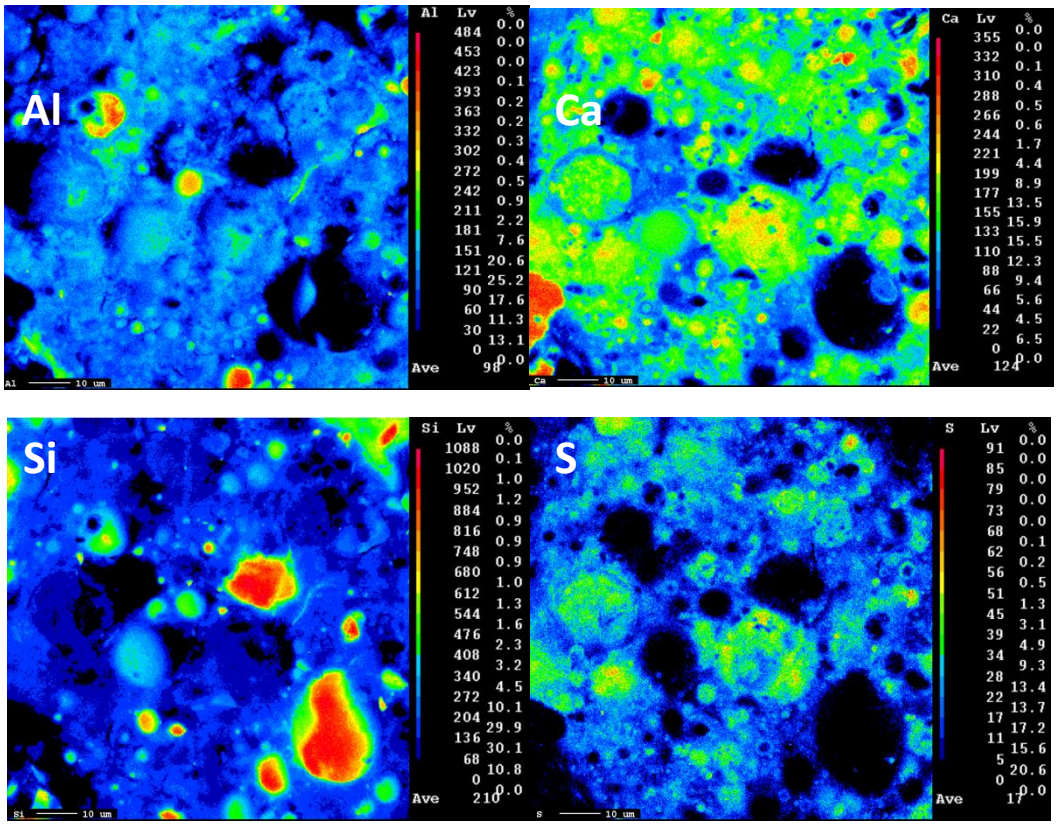

Figure 4.3 Elemental maps (50 × 50 µm, at 0.1 µm/pixel) of a randomly selected site on ordinary fly ash mortar at 28-d

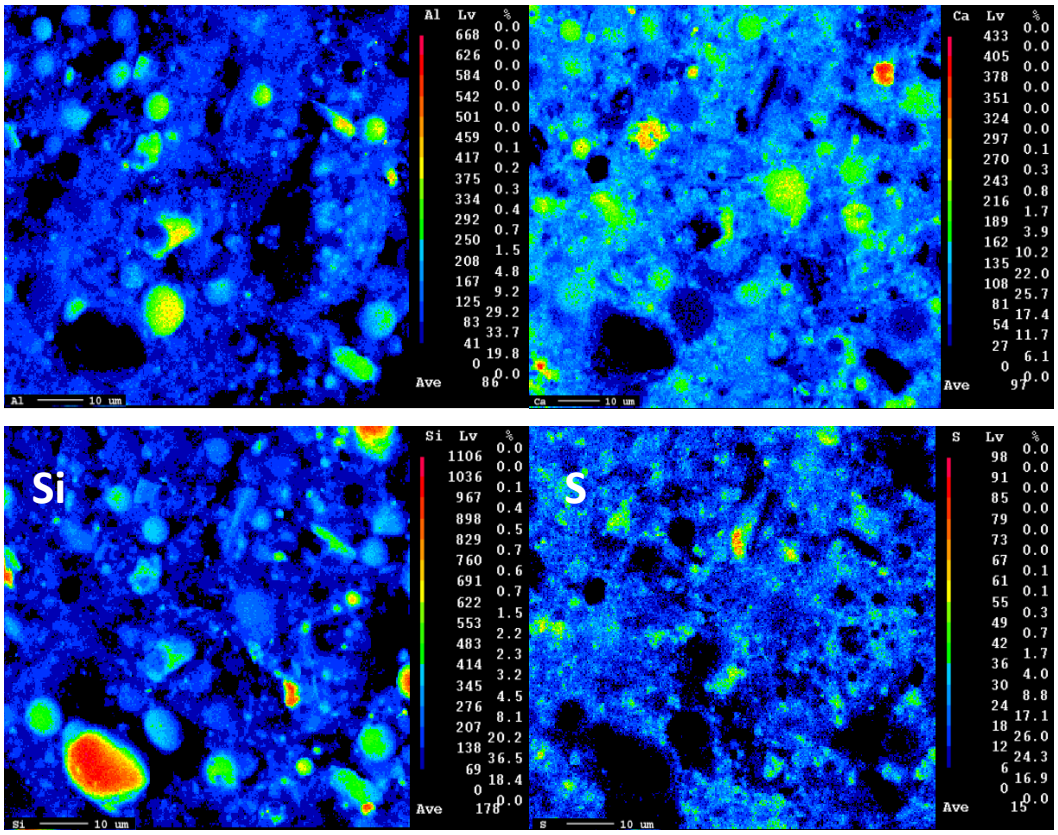

Figure 4.4 Elemental maps (50 × 50 µm, at 0.1 µm/pixel) of a randomly selected site on GO-modified (0.02%) fly ash mortar at 28-d

4.5 Mole Ratio Analysis

The Al/Ca against Si/Ca mole ratio plot was generated for fly ash mortar with/without GO-modification (Fig. 4.5) by processing the electron probe micro-analyzer (EPMA)/wavelength dispersive spectroscopy (WDS) data. One study (Richardson 2000) summarized the elemental mapping data of C-S-H in different pastes (including cement-slag pastes, cement-fly ash pastes, and slag/KOH pastes), and recommended an equation valid for the C-(A)-S-H phase in calcium alumino-silicate cementitious systems.

$$Si/Ca = 0.4277 + (2.366 \text{ X } Al/Ca) \qquad \text{(Equation 1)}$$

This equation is also produced in Fig. 4.5. The phase blending in the fly ash paste at a micron level (≈ 0.01 µm^2) is displayed in these diagrams: The pastes consisted of C-S-H (at

Al/Ca ≈ 0; Si/Ca = 0.5-0.67), $Ca(OH)_2$ (at Si/Ca = 0; Al/Ca = 0), C-(A)-S-H (along the trend line), AFm (at Al/Ca = 0.5, Si/Ca = 0) and AFt (at Al/Ca = 0.33; Si/Ca = 0). A clear pattern is noticed, that most of the hydration phases in the fly ash system were above the proposed C-(A)-S-H composition trend line, revealing that the fly ash system produced more Al-rich hydrates, such as C-A-S-H or C-(A)-S-H with a higher Al substitution. Figure 4.5b shows that GO further facilitated the data separation in three different zones: (1) the Al-rich zone above the C-(A)-S-H trend line; (2) the C-S-H zone; and (3) the jennite zone (confirmed by later NMR results).

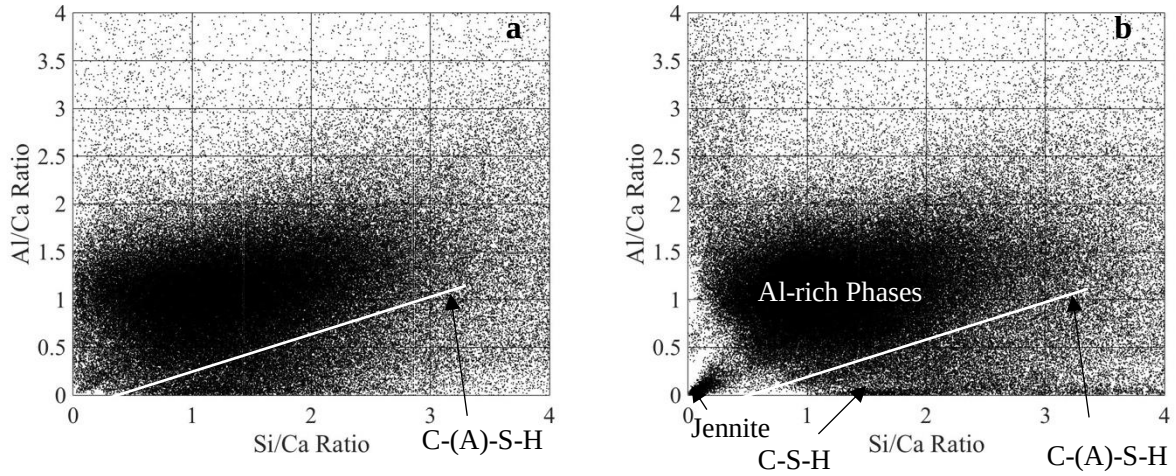

Figure 4.5 Al/Ca against Si/Ca mole ratio plot: (a) fly ash mortar without GO; (b) GO modified fly ash mortar

The phase separation shown in Fig.4.5b strongly suggests that some interactions occurred between hydration precursors and GO. The box plots (Fig. 4.6) of element concentrations were generated from mapping data. Each box-and-whisker represents 500×500 data points. After admixing GO (at 0.01% and 0.02%), the relative distance between the low, median, and upper quartile did not change significantly for all elemental boxplots. However, the position of the box moved upward for Al-concentrations and downward for Ca- and Si-concentrations, suggesting that GO acted primarily as a reduction factor of Ca- and Si-concentration and an increase factor

of Al-concentrations for major fly ash hydrates inside the box, rather than changing their distribution patterns.

Since Ca was mainly present as positively charged ions, it was attracted by electronegative GO sheets and bonded with the "-OH" functional group (Archanjo et al. 2014, Ramesha et al. 2011), resulting in a decrease of Ca-concentration in the pore solution. The influence of GO on the Ca-concentration was reflected in the final hydrates, as the box of Ca-concentration in Fig. 4.6b moved downward with the median reduced by 31% (from 3.20 to 2.21). The Al mainly existed as electronegative tetrahedra (e.g., $Al(OH)^{4-}$), so the negatively charged GO reduced the Al-distribution area in the pore solution through repulsion, resulting in an increase in Al-concentration, which was reflected in the final hydrates as the box of Al-concentration in Fig. 4.6a moved upward with the median increased by 26% (from 2.96 to 3.74). The box of Si-concentration in Fig. 4.6c moved downward slightly with the median reduced by 13% (from 5.39 to 4.71), because GO only affected the electronegative part {$SiO(OH)^{3-}$, $SiO_2(OH)_2^{2-}$} of Si species and had limited influence on neutral $Si(OH)_4^{\circ}$.

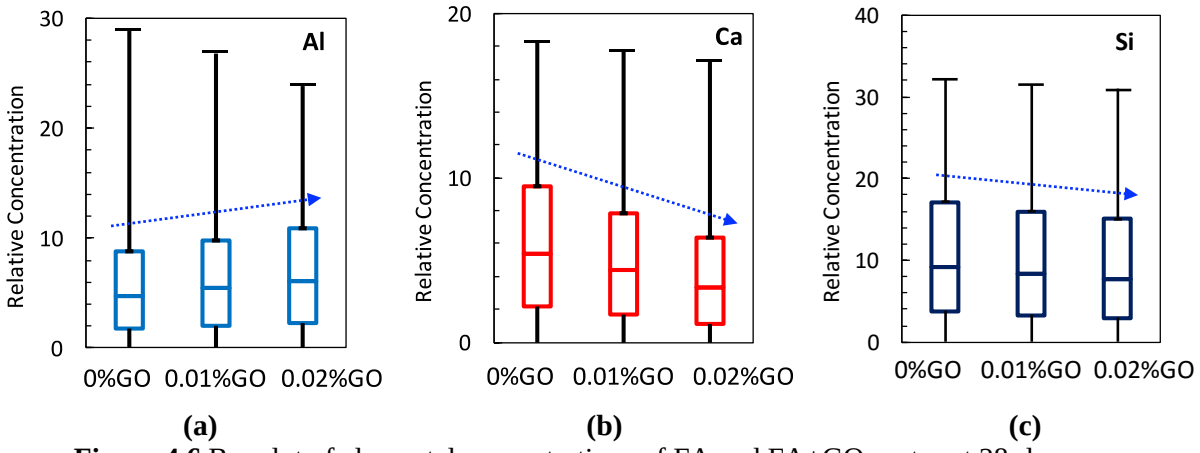

Figure 4.6 Boxplot of elemental concentrations of FA and FA+GO pastes at 28-d: (a) Al; (b) Ca; (c) Si

According to the aforementioned discussion, GO showed the ability to selectively affect the distribution of different hydration precursors: (1) the electronegative GO sheet attracts cationic ions (Ca^{2+}, Na^{+}, K^{+}, and Mg^{2+}) and repels $Al(OH)_4^{-}$ tetrahedra and other electronegative ions; (2) the effect of GO on the Si-distribution was relatively weak because Si existed as both neutral $Si(OH)^4$ units and $SiO(OH)^{3-}$, $SiO_2(OH)_2^{2-}$ anions.

4.6 NMR Study on the Influence of GO

In addition to elemental concentration, the chemical structure and ordering of hydration products are important to elucidate the function of GO in cement hydration. As such, ^{29}Si and ^{27}Al MAS NMR spectroscopy for the Fly Ash and Fly Ash+GO samples at 56 days were performed; the results are presented in Fig. 4.7. $Q^n(mAl)$ notation (n = 0-4, m = 0-n) was used to describe the chemical bonding conditions of Si nuclei in the pastes, where *n* represents the number of adjacent Si linked directly to one Si-tetrahedron and *m* indicates the number of Al substitutions to the adjacent Si (Jeon et al. 2015). Aluminum atoms were categorized into three groups according to the coordinate states, i.e., 4-, 5-, and 6- coordination with oxygen (Jeon et al. 2015). Al(IV), Al(V), and Al(VI) notations were used to indicate these Al coordinates. In Fig. 4.7, each spectrum was semi-quantitatively deconvoluted using a Gaussian function, and the difference between experimental spectra and the sum of components was provided at the bottom of each figure. Table 4.2 provides the peak assignment, integrated area for each deconvoluted component, and references used for the peak assignment.

As shown in Fig. 4.7a,b, after adding GO, the peak area of Q^4 near -112.4 ppm (representing amorphous quartz in fly ash) decreased from 13.2% to 6.3%, suggesting that GO accelerated the fly ash dissolution to provide more precursors for the formation of hydrates (Xu et al. 2017a). Important increases of $Q^1(J)$ (around -81.5 ppm) and Q^4 in low quartz (semi-

crystalline quartz) (Kowalczyk 1992) at -107.4 ppm were marked, indicating that GO promoted the formation of jennite (having higher Ca content than normal C-S-H [Rejmak et al. 2012, Richardson 2004]) and the low quartz phase (the Raman spectra also showed that GO increased the quartz band). Overall, GO increased the total peak area of Q^3 and Q^4 from 47.0% to 54.6%. As such, the polymerization degree of fly ash hydrates was improved by GO.

Figure 4.7c,d show that after adding GO, the intensity of the Al(IV) band decreased, which may have resulted from both the reduction of Al(IV) in fly ash and the reduction of Al(IV) in the AFm interlayer. The former shows that GO accelerated the fly ash dissolution again, and the latter shows that GO could reduce the formation of AFm. The increase of the interlayer Al(V) band in C-S-H can be associated with GO's repulsion, which pushed Al ions into interlayers of C-S-H. The other two peaks of A(VI) remained relatively unchanged.

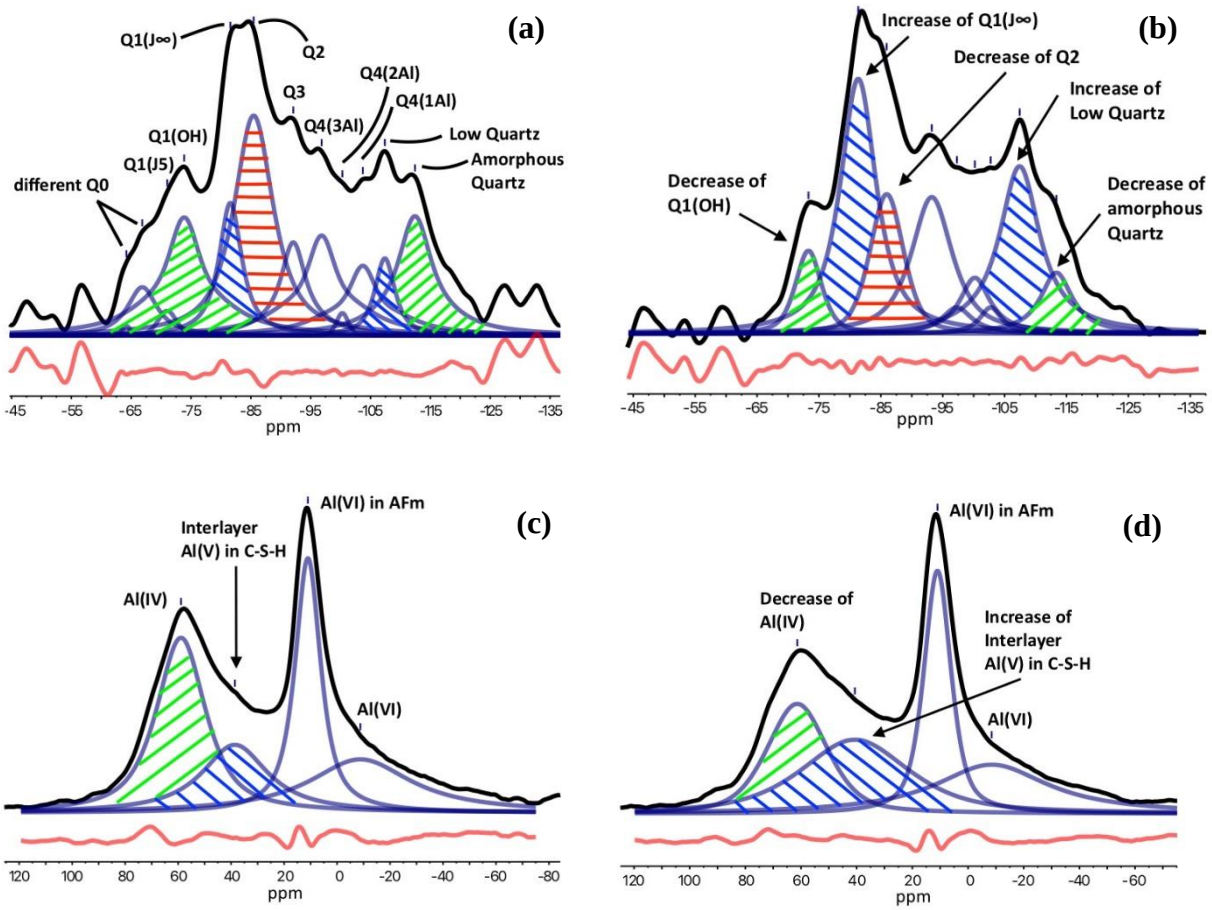

Figure 4.7 29Si MAS NMR spectra at 56-d for (a) FA paste; (b) FA + GO paste, and 27Al MAS NMR spectra for (c) FA paste; (d) FA + GO paste

Table 4.2 Integrated area percentage of deconvoluted NMR spectrum components

Component	Structure	Type	Fly Ash		Fly Ash+GO	
			ppm	area %	ppm	area %
Q^4	3-D network	Q^4 in amorphous	-112.4	13.2	-113.4	6.3
		Q^4 in low quartz	-107.4	4.3	-107.4	21.8
		Q^4(1Al)	-103.7	8.7	-102.7	1.8
		Q^4(2Al)	-100.3	0.6	-100.2	5.5
		Q^4(3Al)	-96.8	12.6	-97.3	2.6
		Sum		39.4		38.0
Q^3	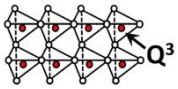	Q^3	-92.1	7.6	-93.2	16.6
		Sum		7.6		16.6
Q^2	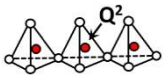	Q^2(0Al)	-85.5	23.6	-85.9	12.0
		Sum		23.6		12.0
Q^1	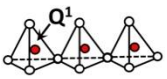	Q^1(J∞)	-81.5	8.6	-81.4	27.6
		Q^1(OH)	-73.9	15.5	-73.3	5.8
		Q^1(J5)	-71.0	1.0	-	-
		Sum		25.1		33.4
Q^0		Different Q^0 units	-66.9	4.1	-	-
			-64.2	0.2	-	-
		Sum		4.3		-
Q^n sum				100		100
Al(IV)		in AFm or fly ash	59.0	32.7	61.4	22.7
Al(V)		Interlayer Al(V) in C-S-H	38.6	18.6	40.6	29.4
Al(VI)		in AFm	11.0	25.6	11.0	23.9
		in C-A-S-H or fly ash	-8.8	23.1	-8.5	24.0
Al(N) sum				100		100

4.7. NMR Coupling with TGA/DTGA

The decrease of the Q^2 band induced by GO (Fig. 4.8a) can be verified by thermogravimetric and differential thermogravimetric analyses (TGA/DTGA). Figure 4.8b displays the average TGA (blue lines) and DTGA (dark lines) curves of three samples per group. The figure reveals that the amount of total C–S–H (first weight loss between 80°C and 200°C) decreased after admixing 0.02 wt% GO, even though this is difficult to estimate as ettringite (main weight loss at 100°C) and AFm (main weight loss at 150°C) overlap the weight loss of C–

S–H. Since Q^2 Si mainly exists in C-S-H chains, it is reasonable to conclude that this decrease in the Q^2 band was related to the C-S-H reduction observed in the TGA/DTGA curves. The weight loss between 600°C and 700°C was assigned to calcite. The weight loss between 700°C and 850°C was from the decomposition of sodium calcium carbonates. Due to the higher content of calcium carbonate and other impurities (e.g., $MgCO_3$) (Bain and Morgan 1969), the peak at 810°C in F+GO samples shifted to a lower temperature at 785°C. Overall, Fig. 4.8b shows that GO increased the resistance to carbonation as the amount of total carbonate (weigth loss between 600°C and 850°C) in GO-modified fly ash pastes was decreased by 6%.

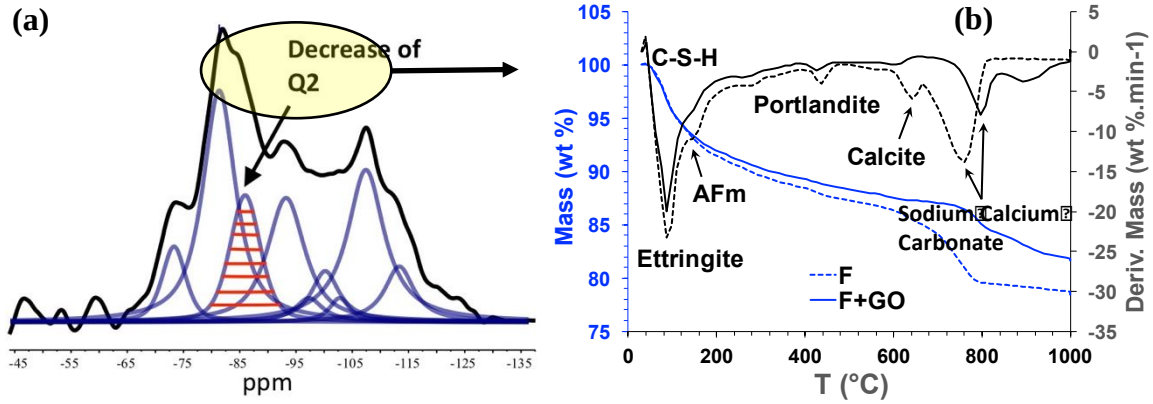

Figure 4.8 Correlation between (a) 29Si MAS NMR spectra and (b) TGA/DTGA, for fly ash pastes at 56-d

4.8 NMR Coupling with XRD and BSE

The increase of Q^4 in low quartz (Fig.4.9a) induced by GO can be verified by X-ray diffraction (XRD). The Crystallography Open Database (http://www.crystallography.net/cod/) was used for this XRD study. Fig. 4.9b shows that akermanite (A), calcite (C), portlandite (CH), ettringite (E), gypsum (G), periclase (P), and quartz (Q) were identified in the hardened fly ash pastes. The intensity of quartz peaks (at 20.86°, 26.62°, 50.18°, and 59.90°) increased noticeably after admixing 0.02 wt% GO in the fly ash pastes. Nuclear magnetic resonance (NMR) results further indicated that this was semi-crystalline quartz (low quartz).

Due to the pre-existing quartz and other quartz-like minerals in the fly ash (Velandia et al. 2016), it was difficult to identify this GO-induced low quartz visually; however, it can be seen in the relatively simple GO-modified cement paste. A typical crystalline appearance in the BSE was identified in the GO-modified cement paste (Fig. 4.9c). Line scans in Fig. 4.9d confirm this was a silica-rich phase, high in Si and low in Al and Ca; a C-plateau was detected with this phase, suggesting this phase was GO-induced and quartz-like. The formation of Si-rich low quartz could be attributed to the absorption of Ca and the repulsion of Al by GO.

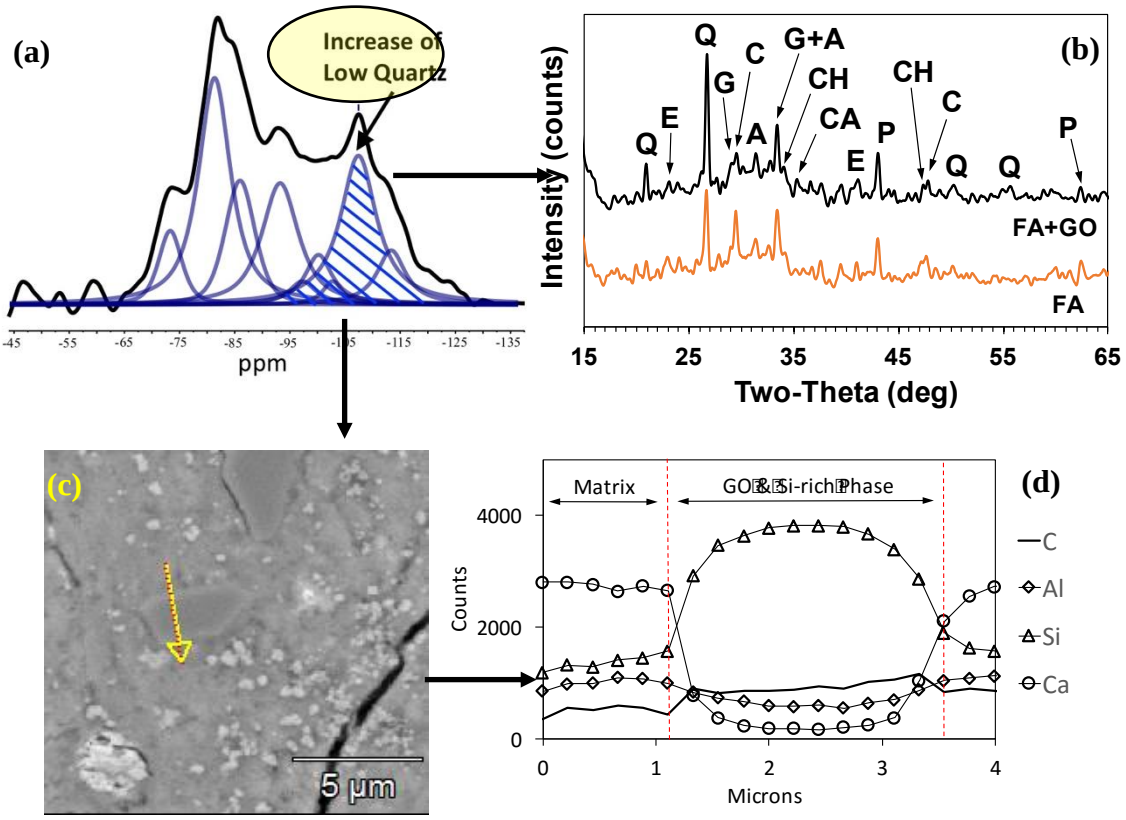

Figure 4.9 Correlation between (a) 29Si MAS NMR spectra and (b) XRD spectra for fly ash pastes at 56-d; (c) BSE image; and (d) elemental line scans of GO-induced quartz-like phase

4.9. NMR Coupling with EPMA and BSE

In Fig.4.10a, the GO-induced increase in $Q^1(J\infty)$, jennite with infinite chain length, had good correlation with EPMA (electron probe microanalysis) data in Fig. 4.10b, where the data

cluster near the origin (low in Al and Si, rich in Ca) were assigned to the jennite phase, as it has a much higher Ca content than normal C-S-H. This phase can be seen in the relatively simple cement paste as well (Fig. 4.10c). The line scans in Fig. 4.10d confirm that the paste was high in Ca and low in Si and Al, and a C-plateau was detected, suggesting this was a GO-induced phase. The formation of jennite could be attributed to the absorption of Ca by GO, which created a local Ca-rich environment.

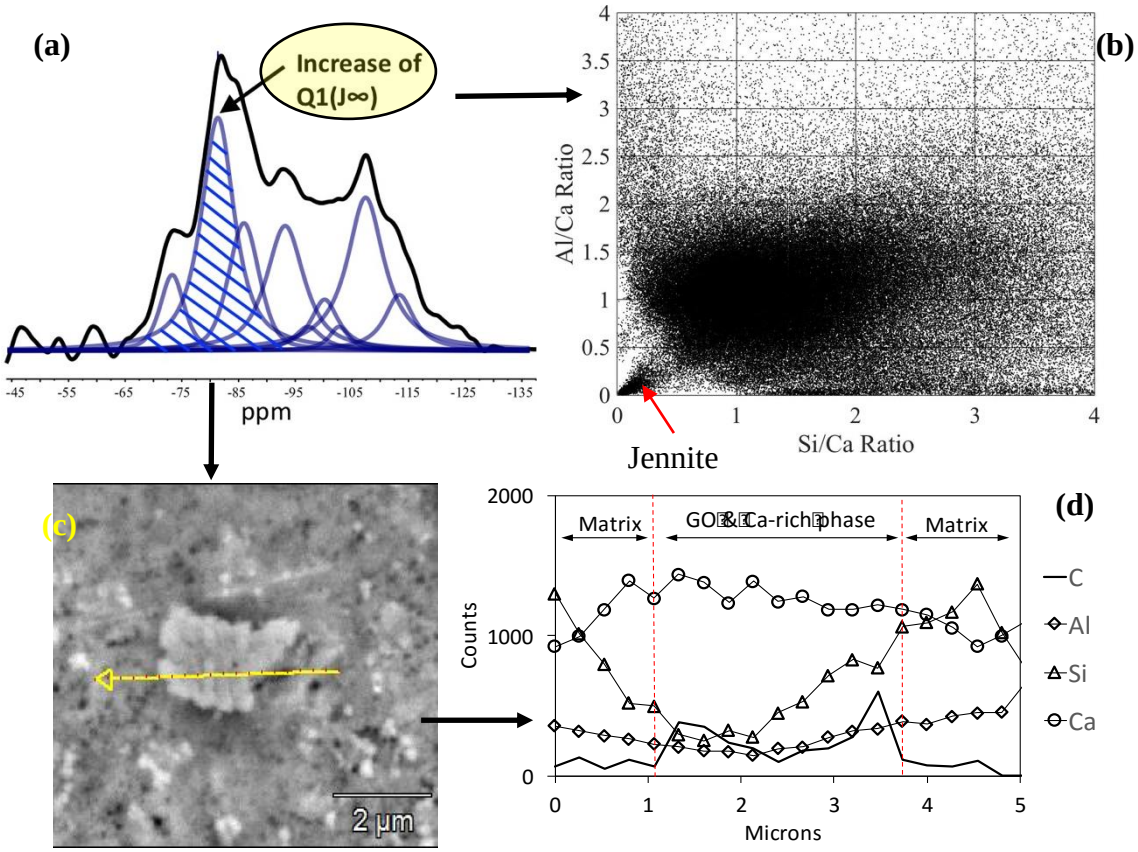

Figure 4.10 Correlation between (a) 29Si MAS NMR spectra; and (b) EMPA data for fly ash pastes at 56-d. (c) BSE image; and (d) elemental line scans of GO-induced jennite phase.

4.10. Fly Ash Hydrates Versus Cement Hydrates in Terms of NMR Spectra

The NMR spectra of fly ash pastes were compared with those of cement pastes. As shown in Fig. 4.11a, fly ash hydrates consisted of 47.0% peak area of network structure (Q^3 and

Q^4) and 23.6% peak area of chain structure (Q^2), so the fly ash binder in this study was essentially a combination of geopolymer binder and cementitious binder. But more than 90% peak area of cement hydrates is on the chain structure (Q^1 and Q^2) side in Fig. 4.11b. Due to the cross-linking three-dimensional network in fly ash hydrates, the structure of fly ash hydrates should be more stable than the linear chain structure of cement hydrates theoretically (Xu et al. 2017a).

The obvious difference is also observed in Al-spectra between fly ash hydrates and cement hydrates (Fig. 4.11c,d). Fly ash hydrates have a significant number of Al(IV) units, either in C-S-H or in unreacted fly ash, and Al(V) units, whereas most Al exists as Al(VI) units in cement hydrates. It can be expected that Al-related durability performance, such as sulfur attack, will be different between fly ash geopolymer and concrete, which merits further study.

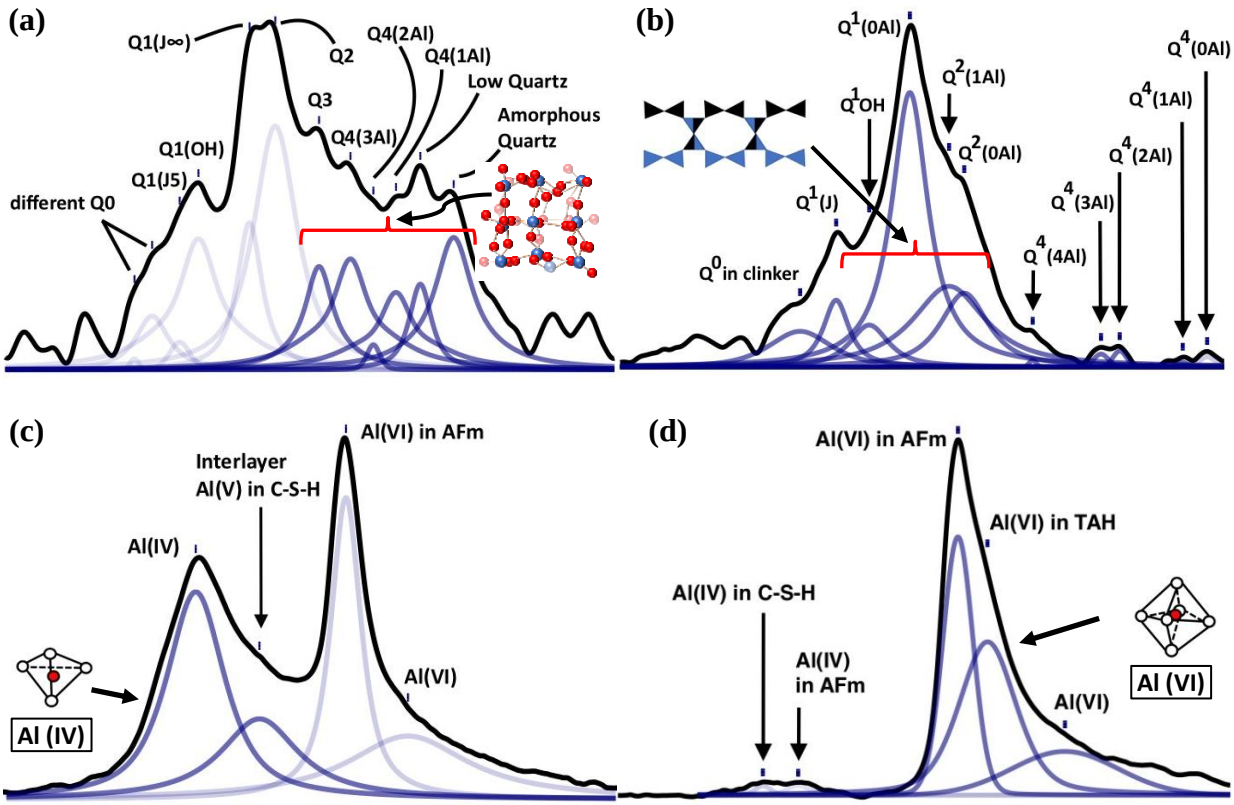

Figure 4.11 29Si MAS NMR spectra for (a) FA paste at 56-d; (b) OPC paste at 56-d, and 27Al MAS NMR spectra for (c) FA paste at 56-d; (d) OPC paste at 56-d.

4.11. Histogram Analysis of Elemental Mole Ratio

Histogram analysis was adopted to study the elemental mole ratio per the function of each element. A summary is presented in Table 4.3. According to the field strength theory (Dietzel 1942), K, Na, and Ca are network modifiers due to their relatively low field strength, and the introduction of these elements into a fly ash geopolymer causes breakage of bridges (O^{2-}). Fe, Al are intermediates and cannot form a network by themselves; network modifiers (K^{+}, Na^{+}, or Ca^{+}) are needed to balance their negative charge. Si is a network former; it can form a SiO_4 tetrahedron, which is the basic building block for geopolymer. As GO showed the ability to selectively affect different sets of elements, it is expected that GO will regulate the mole ratio among different elements.

Table 4.3 Histogram analysis summary of mole ratio mappings

	Ca/Si		Si/Al		S/Ca		Ca/(Si+Al)	
	Mean	**Mode**	**Mean**	**Mode**	**Mean**	**Mode**	**Mean**	**Mode**
FA+GO	0.93	0.45	2.07	0.96	0.23	0.24	0.38	0.32
FA	1.04	0.70	2.78	1.28	0.18	0.26	0.45	0.42

4.11.1. Ca/Si ratio (network modifier / network former)

Due to Ca^{2+} absorption by GO, the bulk average Ca/Si ratio was decreased from 1.04 to 0.93 (by 10%), resulting in the formation of fly ash geopolymer with lower Ca/Si ratios. As shown in Fig.4.12a, the histogram of the Ca/Si ratio further displayed that the GO-modified fly ash sample contained more hydrates at low Ca/Si ratios (Ca/Si < 0.67) than the ordinary fly ash samples, and typical C-S-H with Ca/Si ratio = 0.67~2.0 (Richardson 2014) was less in the GO-modified sample. This reduction in C-S-H was also confirmed in the NMR and TGA results. The superior compressive strength of GO-modified fly ash mortar can be attributed to the increase in bulk Si/Ca ratio, since hydrates with a higher $\frac{\text{network former}}{\text{network modifier}}$ ratio have superior stiffness and hardness (Abdolhosseini Qomi et al. 2014).

4.11.2. Si/Al ratio (network former / intermediate) and S/Ca ratio

The average bulk Si/Al ratio was reduced from 2.78 to 2.07 (by 26%). This reduction can be explained by the repulsion of GO sheets on Al ions in the form of $Al(OH)^{4-}$, which increased the concentration of Al in the pore solutions during hydration, but the influence of GO on Si-concentration was not as great as that of Al. Therefore, GO caused a decrease in the bulk Si/Al ratio. Overall, GO showed an ability to reduce the $\frac{\text{network former}}{\text{intermediate}}$ ratio in fly ash hydrates. Figure 4.12b shows that the peak frequency of the Si/Al ratio at 1.28 shifted towards a lower Si/Al ratio at 0.96 after adding GO.

The histogram of the S/Ca map in Fig. 4.12c shows that the ordinary fly ash sample had higher frequency at S/Ca ≈ 0.25 than the GO-modified fly ash sample, suggesting GO reduced the formation of AFm $\{Ca_4Al_2(SO_4)(OH)_{12}\cdot 6H_2O\}$ with S/Ca=0.25. This AFm reduction at later ages was also confirmed by the NMR results, shown in Table 4.2, as both Al(IV) and Al(VI) units in AFm decreased.

4.11.3. Ca/(Si+Al) ratio (network modifier / network former + intermediate)

The Ca/(Si+Al) ratio (network modifier / network former + intermediate) evaluates the overall network-forming-ability of fly ash geopolymer. The addition of 0.02% GO resulted in a decrease in the bulk average Ca/(Si+Al) ratio from 0.45 to 0.38 (by 15%), implying that GO's uptake of calcium ions led to a decrease of Ca content in the final hydrates. The structure of such hydrates had less degree of Ca^{2+} ion disruption. The Fig. 4.12d histogram of Ca/(Si+Al) map shows that the peak frequency of ordinary fly ash hydrate at Ca/(Si+Al) = 0.42 shifted towards a lower Ca/(Si+Al) ratio at 0.32 after adding GO, suggesting that GO-modified fly ash hydrates tended to form structures with more network formers and less calcium disturbances. As such, GO-modified fly ash hydrates should have better mechanic strength properties.

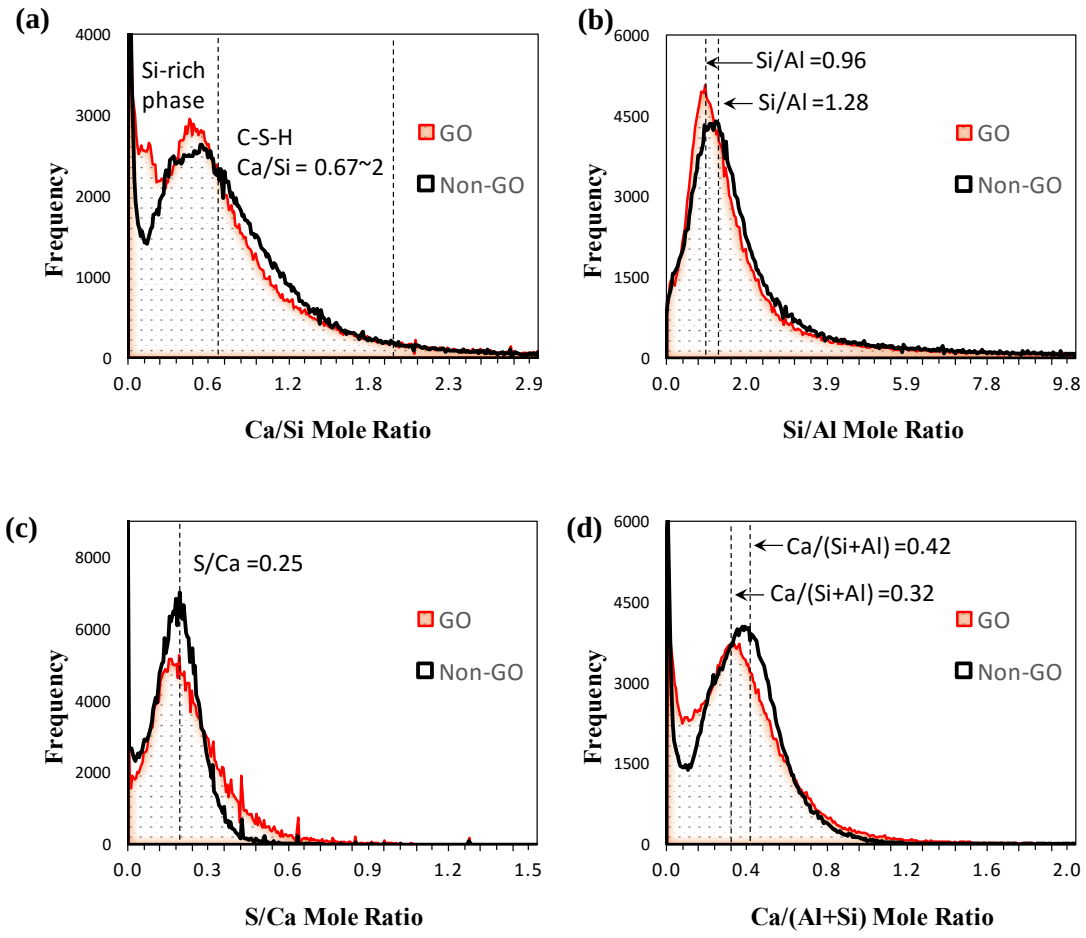

Figure 4.12 Histogram of elemental mole ratio mapping

4.12 Conclusions

The re-engineering of fly ash geopolymer with GO shows promise for improving the strength and durability of fly ash geopolymer. This GO-induced improvement will help divert fly ash from the waste stream toward value-added applications. Fly ash otherwise poses a substantial environmental risk. The findings of this study are expected to contribute to better and broader utilization of GO in fly ash composites. Based on experimental results, the following conclusions have been drawn:

1. The 28-day compressive strength of fly ash geopolymer (cured at room temperature) was increased from 33.6 MPa to 41.4 MPa by adding 0.02% (by weigh of fly ash) GO. The

polymerization degree of fly ash geopolymer was also increased by GO, as the total silica in the form of Q^3 and Q^4 increased from 47.0% to 54.6%. In particular, the amount of Q^4 Si increased from 4.3% to 21.8%.

2. As a functional nanomaterial, GO showed the ability to selectively affect the distribution of different hydration precursors, thereby increasing the compressive strength of fly ash geopolymer, since GO reduces the bulk average Ca/Si and Ca/(Si+Al) ratios of hydrates, and hydrates at lower Ca/Si and Ca/(Si+Al) ratios generally exhibit superior stiffness and hardness. It was found that GO reduced the amount of AFm in fly ash geopolymer.
3. Nuclear magnetic resonance is a powerful tool that can be used to study the chemical ordering and structure of fly ash geopolymer. By cross-referencing NMR, XRD, TGA, and EMPA data, it was found that GO promoted the formation of semi-crystalline quartz and jennite in fly ash hydrates.

CHAPTER 5.0 CONCLUSIONS

5.1 Summary

In this exploratory work, efforts were made to advance scientific knowledge in the utilization of nanotechnology to expand the use of industrial waste and recycled materials in pervious concrete. These efforts included (1) evaluation of the environmental benefits of graphene oxide (GO)-modified fly ash pervious concrete; (2) improvement of the durability performance of GO-modified fly ash pervious concrete at early ages; (3) use of advanced analytical tools to fully characterize GO-modified fly ash binder; and (4) extension of Phase I technology to biomass ash utilization.

Following the Phase I research, the freeze/thaw (F/T) resistance and the ambient-temperature salt resistance of pervious concrete specimens were investigated separately, to isolate the physical and chemical phenomena underlying the deterioration of the specimens during the "salt scaling" test, which combined the effects of F/T cycling and deicer attack. Test results suggest that the incorporation of GO can significantly improve resistance to F/T cycling effects, ambient-temperature salt attack, and "salt scaling" of pervious concrete, for both cement and activated fly ash binder. Graphene-oxide-modified fly ash pervious concrete specimens exhibited the least weight loss during the salt scaling test. This result is partly attributable to the better resistance of the GO-modified hydration products of fly ash as compared with conventional cement hydrates. The specimens were studied using X-ray diffraction and secondary electron imaging tools. Nuclear magnetic resonance (NMR) was employed to examine the degree of polymerization of hydrates. This study provides an enhanced understanding of the F/T and salt scaling resistance of fly ash pervious concrete with or without GO modification.

5.2 Findings

1. Fly ash is a fairly complex material in terms of physical, chemical, and mineralogical properties. The combustion temperature, cooling rate, and composition of fly ash play important roles in determining the physical and cementitious properties of fly ash. High-calcium fly ash is much more complex than low-calcium fly ash in terms of chemical and mineral composition. Due to its low reactivity, low-calcium fly ash has been widely used as a concrete admixture; in the short term, it does not dramatically alter cement hydration chemistry. Recent years have seen an increased use of high-calcium fly ash, based on its growing production. The application of high-calcium fly ash in concrete, however, has been hindered because fly ash can change cement hydration significantly and now lacks its reaction model in concrete. Therefore, more research is needed to support the full use of high-calcium fly ash in concrete.

2. The sustainability of fly ash-based construction materials can be assessed by life cycle assessment (LCA) and cost-benefit analysis (CBA). Alkali-activated fly ash (AAFA) concrete with natural aggregates has the best overall environmental performance despite the high dosage of alkali activators used, and conventional concrete with recycled coarse aggregate (RCA) had the worst performance. But high-volume fly ash concrete with RCA is recommended for in situ applications, as AAFA concrete requires a high curing temperature.

3. Due to the slow hydration of fly ash, the F/T resistance of GO-modified fly ash pervious concrete cured for 28 days was comparable to cement pervious concrete cured for 14 days. Graphene oxide improved the resistance to F/T cycles for both cement and fly ash pervious concretes.

4. Fly ash pervious concrete showed better resistance to NaCl than cement concrete. Compared with the F/T test, which caused rapid physical damage to the pervious concrete

specimens, the salt attack caused slow deterioration in the specimens. Graphene oxide improved the resistance of cement and fly ash pervious concretes to NaCl attack.

5. Graphene oxide promoted the formation of semi-crystalline C–S–H (I) and C-A-S-H gels in fly ash hydrates, which provides better resistance to salt attack.

6. Compared with cement pervious concrete, fly ash pervious concrete showed better reduction factors of sulphate, lead, chloride, total phosphate, and nitrate. Especially for chloride content, fly ash pervious concrete introduced 35% reduction (vs. 19% reduction for cement pervious concrete). Thus, fly ash pervious concrete holds great potential as an effective means of addressing the deicer-laden stormwater issue in cold regions and supports environmental conservation.

7. Graphene oxide showed ability as a functional nanomaterial to selectively affect the distribution of different hydration precursors, and thereby increase the compressive strength of fly ash geopolymer, as GO reduced the bulk average Ca/Si and Ca/(Si+Al) ratios of hydrates. Hydrates at lower Ca/Si and Ca/(Si+Al) ratios generally exhibited superior stiffness and hardness. Graphene oxide was also found to reduce the amount of AFm in fly ash geopolymer.

5.3 Recommendations

Recommendations for future work are proposed as follows:

1. Additional aspects need to be quantified and incorporated into LCA and CBA models to assess the sustainability of fly ash pervious concrete. These aspects include health risks, regulatory compliance, social consensus, and heavy metal leaching risks. Although fly ash-based geopolymers show sustainable benefits in many cases, further endeavor is still needed for large-scale application in the construction industry.

2. Research is needed to better understand the composition, polymerization, and mineral phase of nanomaterial-modified fly ash construction materials. Nuclear magnetic resonance (NMR) testing can be used to quantify the effect of nanomaterials on the polymerization of fly ash hydrates. The ratio of Si Q_n units and the ratio of different Al coordinates can be calculated during the NMR test. X-ray diffraction and XRF should be used to examine the chemical and phase composition of nanomaterial-modified fly ash composites. Field emission electron probe micro-analysis, coupled with scanning electron microscopy, can be used to examine the morphology and elemental ratio. All these advanced tools will shed light on the possible role of nanomaterials in fly ash composites at the micron level, which can improve the performance and sustainability of fly ash-based construction materials.

3. The technology developed for coal fly ash also holds potential for biomass ash solidification. Since biomass is considered a renewable resource and biomass combustion essentially does not contribute to the greenhouse effect due to fast CO_2 conversion, the use of biomass ash in construction materials has significant technological and environmental advantages (Tosti et al. 2018). Consequently, biomass fly ash-based geopolymer is worth exploring.

4. Chemical or mechanical methods can be used to improve the performance of fly ash pervious concrete at early ages. Chemical methods include the use of better activators based on the state of knowledge. Mechanical methods include the use of reinforcing fibers (carbon fibers or plastic fibers) and particles to support the binder matrix.

REFERENCES

Abdolhosseini Qomi, M. J., Krakowiak, K. J., Bauchy, M., Stewart, K. L., Shahsavari, R., Jagannathan, D., Brommer, D. B., Baronnet, A., Buehler, M. J., Yip, S., Ulm, F.-J., Van Vliet, K. J., and Pellenq, R. J.-M. (2014). "Combinatorial molecular optimization of cement hydrates." *Nature Communications*, 5, 4960.

Ahmaruzzaman, M., and Gupta, V. (2012). "Application of coal fly ash in air quality management." *Industrial & Engineering Chemistry Research*, 51(47), 15299–15314.

Amde, A. M., and Rogge, S. (2013). *Development of High Quality Pervious Concrete Specifications for Maryland Conditions*.

Anderson, I., and Dewoolkar, M. M. (2015). "Laboratory freezing-and-thawing durability of fly ash pervious concrete in a simulated field environment." *ACI Materials Journal*, 112(5).

Archanjo, B. S., Araujo, J. R., Silva, A. M., Capaz, R. B., Falcão, N. P. S., Jorio, A., and Achete, C. A. (2014). "Chemical analysis and molecular models for calcium–oxygen–carbon interactions in black carbon found in fertile Amazonian anthrosoils." *Environmental Science & Technology*, 48(13), 7445–7452.

ASTM C192/C192M. (2016). *Standard Practice for Making and Curing Concrete Test Specimens in the Laboratory*. ASTM International, West Conshohocken, PA, 8.

ASTM C215-14. (2014). *Standard Test Method for Fundamental Transverse, Longitudinal, and Torsional Resonant Frequencies of Concrete Specimens*. ASTM International, West Conshohocken, PA, 7.

ASTM C666 / C666M-15. (2015). *Standard Test Method for Resistance of Concrete to Rapid Freezing and Thawing*. ASTM International, West Conshohocken, PA, 7.

Azfar, I. (2009). *Evaluation of Pervious Concrete as a Best Management Practice for Stormwater in Edwards Aquifer Region*. ProQuest.

Bae, S., Meral, C., Oh, J., Moon, J., Kunz, M., and Monteiro, P. J. M. (2014). "Characterization of morphology and hydration products of high-volume fly ash paste by monochromatic scanning x-ray micro-diffraction (μ-SXRD)." *Cement and Concrete Research*, 59, 155–164.

Bain, J. A., and Morgan, D. J. (1969). "The role of thermal analysis in the evaluation of impure clay deposits as mineral raw materials." *Clay Minerals*, 8(2), 171–192.

Bakharev, T. (2005). "Geopolymeric materials prepared using Class F fly ash and elevated temperature curing." *Cement and Concrete Research*, 35(6), 1224–1232.

Balaguera, A., Carvajal, G. I., Albertí, J., and Fullana-i-Palmer, P. (2018). "Life cycle assessment of road construction alternative materials: A literature review." *Resources, Conservation and Recycling*, 132, 37–48.

Berry, M., Stephens, J., and Cross, D. (2011). "Performance of 100% fly ash concrete with recycled glass aggregate." *ACI Materials Journal*, 108(4), 378–384.

Bodor, M., Santos, R. M., Cristea, G., Salman, M., Cizer, Ö., Iacobescu, R. I., Chiang, Y. W., van Balen, K., Vlad, M., and van Gerven, T. (2016). "Laboratory investigation of carbonated BOF slag used as partial replacement of natural aggregate in cement mortars." *Cement and Concrete Composites*, 65, 55–66.

Brouwers, H. J. H., and Van Eijk, R. J. (2002). "Fly ash reactivity: extension and application of a shrinking core model and thermodynamic approach." *Journal of materials science*, 37(10), 2129–2141.

Brouwers, H. J. H., and Eijk, V. R. J. (2003). "Chemical reaction of fly ash." *Proceedings of the 11th International Congress on the Chemistry of Cement (ICCC)*, Durban, South Africa.

C09 Committee. (2012). *Specification for Coal Fly Ash and Raw or Calcined Natural Pozzolan for Use in Concrete*. ASTM International.

Chi, M., and Huang, R. (2013). "Binding mechanism and properties of alkali-activated fly ash/slag mortars." *Construction and Building Materials*, Special Section on Recycling Wastes for Use as Construction Materials, 40, 291–298.

Chindaprasirt, P., and Chalee, W. (2014). "Effect of sodium hydroxide concentration on chloride penetration and steel corrosion of fly ash-based geopolymer concrete under marine site." *Construction and Building Materials*, 63, 303–310.

Criado, M., Fernández-Jiménez, A., and Palomo, A. (2010). "Alkali activation of fly ash. Part III: Effect of curing conditions on reaction and its graphical description." *Fuel*, 89(11), 3185–3192.

Darwin, D., Browning, J., Gong, L., and Hughes, S. R. (2008). "Effects of deicers on concrete deterioration." *ACI Materials Journal*, 105(6), 622–627.

Demirbas, A. (2005). "Potential applications of renewable energy sources, biomass combustion problems in boiler power systems and combustion related environmental issues." *Progress in Energy and Combustion Science*, 31(2), 171–192.

Deventer, J. S. J. van, Nicolas, R. S., Ismail, I., Bernal, S. A., Brice, D. G., and Provis, J. L. (2015). "Microstructure and durability of alkali-activated materials as key parameters for standardization." *Journal of Sustainable Cement-Based Materials*, 4(2), 116–128.

Dierkes, C, Göbel, P, Benze, W, and Wells, J. (2000). "Next generation water sensitive stormwater management techniques. In: Melbourne Water." *Proceedings of the Second National Conference on Water Sensitive Urban Design*, Brisbane, Australia.

Dietzel, A. (1942). "The cation field strengths and their relation to devitrifying processes, to compound formation and to the melting points of silicates." *Z. Elektrochem. Angew. Phys. Chemie.*, (48), 9–23.

Dimas, D., Giannopoulou, I., and Panias, D. (2009). "Polymerization in sodium silicate solutions: a fundamental process in geopolymerization technology." *Journal of Materials Science*, 44(14), 3719–3730.

Duan, P., Yan, C., and Zhou, W. (2017). "Compressive strength and microstructure of fly ash based geopolymer blended with silica fume under thermal cycle." *Cement and Concrete Composites*, 78, 108–119.

Dunstan, E. R. J. (1989). *Ash-in-Concrete Model Development: Final Report*. Electric Power Research Inst., Palo Alto, CA (USA); Dunstan, Inc., Lakewood, CO (USA).

Dutta, P. K., and Shieh, D.-C. (1985). "Raman spectral study of the composition of basic silicate solutions." *Applied Spectroscopy*, 39(2), 343–346.

Enders, M. (1995). "Microanalytical characterization (AEM) of glassy spheres and anhydrite from a high-calcium lignite fly ash from Germany." *Cement and Concrete Research*, 25(6), 1369–1377.

Fan, W.-J., Wang, X.-Y., and Park, K.-B. (2015). "Evaluation of the chemical and mechanical properties of hardening high-calcium fly ash blended concrete." *Materials*, 8(9), 5933–5952.

Fernández-Jiménez, A., and Palomo, A. (2003). "Characterisation of fly ashes. Potential reactivity as alkaline cements☆." *Fuel*, 82(18), 2259–2265.

Fernandez-Jimenez, A., García-Lodeiro, I., and Palomo, A. (2006). "Durability of alkali-activated fly ash cementitious materials." *Journal of Materials Science*, 42(9), 3055–3065.

Freidin, C. (1999). "Hydration and strength development of binder based on high-calcium oil shale fly ash: Part II. Influence of curing conditions on long-term stability." *Cement and Concrete Research*, 29(11), 1713–1719.

Garcia-Lodeiro, I., Palomo, A., Fernández-Jiménez, A., and Macphee, D. E. (2011). "Compatibility studies between N-A-S-H and C-A-S-H gels. Study in the ternary diagram Na2O–CaO–Al2O3–SiO2–H2O." *Cement and Concrete Research*, 41(9), 923–931.

Garcia-Lodeiro, I., Fernandez-Jimenez, A., and Palomo, A. (2013a). "Hydration kinetics in hybrid binders: Early reaction stages." *Cement and Concrete Composites*, 39, 82–92.

García-Lodeiro, I., Fernández-Jiménez, A., and Palomo, A. (2013b). "Variation in hybrid cements over time. Alkaline activation of fly ash–portland cement blends." *Cement and Concrete Research*, 52, 112–122.

Garcia-Lodeiro, I., Donatello, S., Fernández-Jiménez, A., and Palomo, Á. (2016). "Hydration of hybrid alkaline cement containing a very large proportion of fly ash: A descriptive model." *Materials*, 9(7), 605.

Garg, N., Wang, K., and Martin, S. W. (2013). "A Raman spectroscopic study of the evolution of sulfates and hydroxides in cement–fly ash pastes." *Cement and Concrete Research*, 53, 91–103.

Gonen, T., and Yazicioglu, S. (2007). "The influence of mineral admixtures on the short and long-term performance of concrete." *Building and Environment*, 42(8), 3080–3085.

Gong, K., Pan, Z., Korayem, A. H., Qiu, L., Li, D., Collins, F., Wang, C. M., and Duan, W. H. (2015). "Reinforcing effects of graphene oxide on Portland cement paste." *Journal of Materials in Civil Engineering*, 27(2).

Gout, R., Pokrovski, G. S., Schott, J., and Zwick, A. (2000). "Raman spectroscopic study of aluminum silicate complexes at 20°C in basic solutions." *Journal of Solution Chemistry*, 29(12), 1173–1186.

Gress, D. (1997). “Early distress in concrete pavements.”

Guo, X., Shi, H., and Dick, W. A. (2010). “Compressive strength and microstructural characteristics of class C fly ash geopolymer.” *Cement and Concrete Composites*, 32(2), 142–147.

Harwalkar, A., and Awanti, S. (2014). “Laboratory and field investigations on high-volume fly ash concrete for rigid pavement.” *Transportation Research Record: Journal of the Transportation Research Board*, 2441, 121–127.

Horner, R. R., Skupien, J. J., Livingston, E. H., and Shaver, H. E. (1994). *Fundamentals of urban runoff management—Technical and institutional issues*. Terrene Institute, Washington, DC.

Hossain, M. U., Poon, C. S., Lo, I. M. C., and Cheng, J. C. P. (2017). “Comparative LCA on using waste materials in the cement industry: A Hong Kong case study.” *Resources, Conservation and Recycling*, 120, 199–208.

Huang, T. Y., Chiueh, P. T., and Lo, S. L. (2017a). “Life-cycle environmental and cost impacts of reusing fly ash.” *Resources, Conservation and Recycling*, 123, 255–260.

Huang, T. Y., Chiueh, P. T., and Lo, S. L. (2017b). “Life-cycle environmental and cost impacts of reusing fly ash.” *Resources, Conservation and Recycling*, 123, 255–260.

Hunt, J. D., Kavner, A., Schauble, E. A., Snyder, D., and Manning, C. E. (2011). “Polymerization of aqueous silica in H2O–K2O solutions at 25–200°C and 1bar to 20kbar.” *Chemical Geology*, 283(3–4), 161–170.

Illikainen, M., Tanskanen, P., Kinnunen, P., Körkkö, M., Peltosaari, O., Wigren, V., Österbacka, J., Talling, B., and Niinimäki, J. (2014). “Reactivity and self-hardening of fly ash from the fluidized bed combustion of wood and peat.” *Fuel*, 135, 69–75.

Iribarne, J., Iribarne, A., Blondin, J., and Anthony, E. J. (2001). “Hydration of combustion ashes — A chemical and physical study.” *Fuel*, 80(6), 773–784.

Ismail, I., Bernal, S. A., Provis, J. L., Hamdan, S., and Deventer, J. S. J. van. (2013a). “Microstructural changes in alkali activated fly ash/slag geopolymers with sulfate exposure.” *Materials and Structures*, 46(3), 361–373.

Ismail, I., Bernal, S. A., Provis, J. L., San Nicolas, R., Brice, D. G., Kilcullen, A. R., Hamdan, S., and van Deventer, J. S. J. (2013b). “Influence of fly ash on the water and chloride permeability of alkali-activated slag mortars and concretes.” *Construction and Building Materials*, 48, 1187–1201.

ISO. (2006). *ISO 14040:2006(en), Environmental management — Life cycle assessment — Principles and framework*. International Organization for Standardization, Geneva.

Jeon, D., Jun, Y., Jeong, Y., and Oh, J. E. (2015). “Microstructural and strength improvements through the use of Na2CO3 in a cementless Ca(OH)2-activated Class F fly ash system.” *Cement and Concrete Research*, 67, 215–225.

Joung, Y. (2008). “Evaluation and optimization of pervious concrete with respect to permeability and clogging.” Texas A&M University.

Kloprogge, J. T., Wharton, D., Hickey, L., and Frost, R. L. (2002). “Infrared and Raman study of interlayer anions CO32−, NO3−, SO42− and ClO4− in Mg/Al-hydrotalcite.” *American Mineralogist*, 87(5–6), 623–629.

Kowalczyk, G. E. (1992). “Quantitative determination of crystalline silica utilizing solid state silicon-29 NMR.”

Kutchko, B. G., and Kim, A. G. (2006). “Fly ash characterization by SEM–EDS.” *Fuel*, 85(17–18), 2537–2544.

Kwon, S.-J., Lee, H.-S., Karthick, S., Saraswathy, V., and Yang, H.-M. (2017). “Long-term corrosion performance of blended cement concrete in the marine environment – A real-time study.” *Construction and Building Materials*, 154, 349–360.

Law, D. W., Adam, A. A., Molyneaux, T. K., Patnaikuni, I., and Wardhono, A. (2015). “Long term durability properties of class F fly ash geopolymer concrete | SpringerLink.” *Materials and Structures*, 48(3), 721–731.

Lee, C., Wei, X., Kysar, J. W., and Hone, J. (2008). “Measurement of the elastic properties and intrinsic strength of monolayer graphene.” *Science*, 321(5887), 385–388.

Lee, C. Y., Lee, H. K., and Lee, K. M. (2003). “Strength and microstructural characteristics of chemically activated fly ash–cement systems.” *Cement and Concrete Research*, 33(3), 425–431.

Lee, H., Cody, R. D., Cody, A. M., and Spry, P. G. (2000). “Effects of various deicing chemicals on pavement concrete deterioration.” *Mid-Continente Transportation Symposium Proceedings*, 151–155.

Lee, M.-G., Tia, M., Chuang, S.-H., Huang, Y., and Chiang, C.-L. (2014). “Pollution and purification study of the pervious concrete pavement material.” *Journal of Materials in Civil Engineering*, 26(8), 04014035.

Li, C. (2011). “Research on the glass phase of slag, high calcium fly ash and low calcium fly ash and their hydration mechanism.” Doctor of Engineering, Tsinghua University.

Li, C., Sun, H., and Li, L. (2010). “A review: The comparison between alkali-activated slag (Si + Ca) and metakaolin (Si + Al) cements.” *Cement and Concrete Research*, 40(9), 1341–1349.

Li, D., Mueller, M. B., Gilje, S., Kaner, R. B., and Wallace, G. G. (2008). “Processable aqueous dispersions of graphene nanosheets.” *Nature nanotechnology*, 3(2), 101–105.

Li, G. (2004). “Properties of high-volume fly ash concrete incorporating nano-SiO2.” *Cement and Concrete Research*, 34(6), 1043–1049.

Liu, F., Sun, Z., and Qi, C. (2015). “Raman spectroscopy study on the hydration behaviors of Portland cement pastes during setting.” *Journal of Materials in Civil Engineering*, 27(8), 04014223.

Lothenbach, B., Scrivener, K., and Hooton, R. D. (2011). “Supplementary cementitious materials.” *Cement and Concrete Research*, 41(12), 1244–1256.

Lv, S., Ting, S., Liu, J., and Zhou, Q. (2014). “Use of graphene oxide nanosheets to regulate the microstructure of hardened cement paste to increase its strength and toughness.” *CrystEngComm,* 16(36), 8508–8516.

Marchand, J., Pigeon, M., Bager, D., and Talbot, C. (1999). “Influence of chloride solution concentration on deicer salt scaling deterioration of concrete.” *Materials Journal,* 96(4), 429–435.

Marinković, S., Dragaš, J., Ignjatović, I., and Tošić, N. (2017). “Environmental assessment of green concretes for structural use.” *Journal of Cleaner Production*, 154, 633–649.

McCarthy, G. J., and Solem-Tishmack, J. K. (1994). “Hydration mineralogy of cementitious coal combustion by-products.” ASCE, 103–121.

Mehta, P. K. (1984). “Testing and correlation of fly ash properties with respect to pozzolanic behavior.”

Merlino, S., Bonaccorsi, E., and Armbruster, T. (1999). “Tobermorites: Their real structure and order-disorder (OD) character.” *American Mineralogist,* 84(10), 1613–1621.

Minkara, R. (2015). “Beneficial use of ash in concrete.” Raleigh, NC.

Mo, L., Zhang, F., Panesar, D. K., and Deng, M. (2016). “Development of low-carbon cementitious materials via carbonating Portland cement–fly ash–magnesia blends under various curing scenarios: A comparative study.” *Journal of Cleaner Production*.

Naik, T. R., Ramme, B. W., Kraus, R. N., and Siddique, R. (2003). “Long-term performance of high-volume fly ash concrete pavements.” *Materials Journal,* 100(2), 150–155.

Nasvi, M. C. M., Ranjith, P. G., and Sanjayan, J. (2013). “The permeability of geopolymer at down-hole stress conditions: Application for carbon dioxide sequestration wells.” *Applied Energy,* Special Issue on Advances in Sustainable Biofuel Production and Use. XIX International Symposium on Alcohol Fuels – ISAF, 102, 1391–1398.

Nurgesang, F. A., Wattanasiriwech, S., Wattanasiriwech, D., and Aungkavattana, P. (2016). “Mechanical and physical properties of fly ash geopolymer-mullite composites.” *Suranaree Journal of Science & Technology*, 23(1).

Oey, T., Bullard, J., Stutzmann, P., Zhao, M., Kumar, A., Bauchy, M., and Sant, G. (2015). “Linking fly ash composition to performance in cementitious systems.” Nasvhile, TN.

Okoye, F. N., Prakash, S., and Singh, N. B. (2017). “Durability of fly ash based geopolymer concrete in the presence of silica fume.” *Journal of Cleaner Production,* 149, 1062–1067.

Olivia, M., and Nikraz, H. (2012). “Properties of fly ash geopolymer concrete designed by Taguchi method.” *Materials & Design*, Sustainable Materials, Design and Applications, 36, 191–198.

Ortega, J. M., Esteban, M. D., Rodríguez, R. R., Pastor, J. L., Ibanco, F. J., Sánchez, I., and Climent, M. Á. (2017). “Long-term behaviour of fly ash and slag cement grouts for micropiles exposed to a sulphate aggressive medium.” *Materials,* 10(6), 598.

Palomo, A., Grutzeck, M. W., and Blanco, M. T. (1999). “Alkali-activated fly ashes: A cement for the future.” *Cement and Concrete Research*, 29(8), 1323–1329.

Palomo, A., Fernández-Jiménez, A., Kovalchuk, G., Ordoñez, L. M., and Naranjo, M. C. (2007). "Opc-fly ash cementitious systems: study of gel binders produced during alkaline hydration." *Journal of Materials Science*, 42(9), 2958–2966.

Poinot, T., Laracy, M. E., Aponte, C., Jennings, H. M., Ochsendorf, J. A., and Olivetti, E. A. (2018). "Beneficial use of boiler ash in alkali-activated bricks." *Resources, Conservation and Recycling*, 128, 1–10.

Potgieter-Vermaak, S. S., Potgieter, J. H., Belleil, M., DeWeerdt, F., and Van Grieken, R. (2006). "The application of Raman spectrometry to the investigation of cement: Part II: A micro-Raman study of OPC, slag and fly ash." *Cement and Concrete Research*, 36(4), 663–670.

Ramesha, G. K., Vijaya Kumara, A., Muralidhara, H. B., and Sampath, S. (2011). "Graphene and graphene oxide as effective adsorbents toward anionic and cationic dyes." *Journal of Colloid and Interface Science*, 361(1), 270–277.

Ramezanianpour, A. A. (2014). "Fly Ash." *Cement Replacement Materials*, Springer Berlin Heidelberg, Berlin, Heidelberg, 47–156.

Ranjbar, N., Mehrali, M., Mehrali, M., Alengaram, U. J., and Jumaat, M. Z. (2015). "Graphene nanoplatelet-fly ash based geopolymer composites." *Cement and Concrete Research*, 76, 222–231.

Rashad, A. M. (2014). "A comprehensive overview about the influence of different admixtures and additives on the properties of alkali-activated fly ash." *Materials & Design*, 53, 1005–1025.

Rejmak, P., Dolado, J. S., Stott, M. J., and Ayuela, A. (2012). "^{29} Si NMR in Cement: A Theoretical Study on Calcium Silicate Hydrates." *The Journal of Physical Chemistry C*, 116(17), 9755–9761.

Richardson, I. G. (2000). "The nature of the hydration products in hardened cement pastes." *Cement and Concrete Composites*, 22(2), 97–113.

Richardson, I. G. (2004). "Tobermorite/jennite- and tobermorite/calcium hydroxide-based models for the structure of C-S-H: Applicability to hardened pastes of tricalcium silicate, β-dicalcium silicate, Portland cement, and blends of Portland cement with blast-furnace slag, metakaolin, or silica fume." *Cement and Concrete Research*, H. F. W. Taylor Commemorative Issue, 34(9), 1733–1777.

Richardson, I. G. (2014). "Model structures for C-(A)-S-H(I)." *Acta Crystallographica Section B: Structural Science, Crystal Engineering and Materials*, 70(6), 903–923.

Richardson, I. G., Girão, A. V., Taylor, R., and Jia, S. (2016). "Hydration of water- and alkali-activated white Portland cement pastes and blends with low-calcium pulverized fuel ash." *Cement and Concrete Research*, 83, 1–18.

Roskos, C. (2011). "Building Green: Development and evaluation of an environmentally friendly concrete." Masters of Science, Montana State University.

Roy, D. M. (1999). "Alkali-activated cements opportunities and challenges." *Cement and Concrete Research*, 29(2), 249–254.

Saafi, M., Tang, L., Fung, J., Rahman, M., and Liggat, J. (2015). “Enhanced properties of graphene/fly ash geopolymeric composite cement.” *Cement and Concrete Research*, 67, 292–299.

Schaefer, V. R., Suleiman, M. T., Wang, K., Kevern, J. T., and Wiegand, P. (2006a). “An overview of pervious concrete applications in stormwater management and pavement systems.” *Civil, Construction and Environmental Engineering, Iowa State University, Ames, IA*, 50011.

Schaefer, V. R., Wang, K., Suleiman, M. T., and Kevern, J. T. (2006b). *Mix Design Development for Pervious Concrete In Cold Weather Climates*. Iowa State University.

Schmidt, M., Fehling, E., and Glotzbach, C. (2012). *Ultra-High Performance Concrete and Nanotechnology in Construction. Proceedings of Hipermat 2012. 3rd International Symposium on UHPC and Nanotechnology for High Performance Construction Materials*. kassel university press GmbH.

Schneider, M., Romer, M., Tschudin, M., and Bolio, H. (2011). “Sustainable cement production—present and future.” *Cement and Concrete Research*, Special Issue: 13th International Congress on the Chemistry of Cement, 41(7), 642–650.

Šefčík, J., and McCormick, A. V. (1997). “Thermochemistry of aqueous silicate solution precursors to ceramics.” *AIChE Journal*, 43(S11), 2773–2784.

Seo, M. W., Goo, J. H., Kim, S. D., Lee, S. H., and Choi, Y. C. (2010). “Gasification characteristics of coal/biomass blend in a dual circulating fluidized bed reactor.” *Energy & Fuels*, 24(5), 3108–3118.

Seto, K. E., Churchill, C. J., and Panesar, D. K. (2017). “Influence of fly ash allocation approaches on the life cycle assessment of cement-based materials.” *Journal of Cleaner Production*, 157, 65–75.

Sheng, G., Li, Q., and Zhai, J. (2012). “Investigation on the hydration of CFBC fly ash.” *Fuel*, 98, 61–66.

Sheng, G., Li, Q., Zhai, J., and Li, F. (2007). “Self-cementitious properties of fly ashes from CFBC boilers co-firing coal and high-sulphur petroleum coke.” *Cement and Concrete Research*, 37(6), 871–876.

Shi, X., Akin, M., Pan, T., Fay, L., Liu, Y., and Yang, Z. (2009). “Deicer impacts on pavement materials: Introduction and recent developments.” *The Open Civil Engineering Journal*, 3(1), 16–27.

Shi, X., Quilty, S. M., Long, T., Jayakaran, A., Fay, L., and Xu, G. (2017). “Managing airport stormwater containing deicers: Challenges and opportunities.” *Frontiers of Structural and Civil Engineering*, 11(1), 35–46.

Šiler, P., Bayer, P., Sehnal, T., Kolářová, I., Opravil, T., and Šoukal, F. (2015). “Effects of high-temperature fly ash and fluidized bed combustion ash on the hydration of Portland cement.” *Construction and Building Materials*, 78, 181–188.

Song, Y., Guo, C., Qian, J., and Ding, T. (2015). “Effect of the Ca-to-Si ratio on the properties of autoclaved aerated concrete containing coal fly ash from circulating fluidized bed combustion boiler.” *Construction and Building Materials*, 83, 136–142.

Stutzxnan, P. E., and Centeno, L. (1995). *Compositional Analysis of Beneficiated Fly Ashes*. NISTIR.

Sugama, T., Brothers, L. E., and Van de Putte, T. R. (2005). "Acid-resistant cements for geothermal wells: sodium silicate activated slag/fly ash blends." *Advances in Cement Research*, 17(2), 65–75.

Sushil, S., and Batra, V. S. (2006). "Analysis of fly ash heavy metal content and disposal in three thermal power plants in India." *Fuel*, 85(17–18), 2676–2679.

Swaddle, T. (2001). "Silicate complexes of aluminum(III) in aqueous systems." *Coordination Chemistry Reviews*, 219–221, 665–686.

Swaddle, T. W., Salerno, J., and Tregloan, P. A. (1994). "Aqueous aluminates, silicates, and aluminosilicates." *Chemical Society Reviews*, 23(5), 319–325.

Thomas, M. D. A. (2007). *Optimizing the Use of Fly Ash in Concrete*. Portland Cement Association Skokie, IL.

Thomas, M. D. A., and Bamforth, P. B. (1999). "Modelling chloride diffusion in concrete: Effect of fly ash and slag." *Cement and Concrete Research*, 29(4), 487–495.

"Thomas Telford Bookshop – Civil Engineering Publications." (n.d.). <http://www.thomastelford.com/books/bookshop_main.asp?ISBN=9780727725929> (Aug. 15, 2017).

Tishmack, J. K., Olek, J., and Diamond, S. (1999). "Characterization of high-calcium fly ashes and their potential influence on ettringite formation in cementitious systems." *Cement Concrete and Aggregates*, 21(1), 82–92.

Tishmack, J. K., Olek, J., Diamond, S., and Sahu, S. (2001). "Characterization of pore solutions expressed from high-calcium fly-ash–water pastes." *Fuel*, 80(6), 815–819.

Tosti, L., van Zomeren, A., Pels, J. R., and Comans, R. N. J. (2018). "Technical and environmental performance of lower carbon footprint cement mortars containing biomass fly ash as a secondary cementitious material." *Resources, Conservation and Recycling*, 134, 25–33.

Tosun-Felekoğlu, K., Gödek, E., Keskinateş, M., and Felekoğlu, B. (2017). "Utilization and selection of proper fly ash in cost effective green HTPP-ECC design." *Journal of Cleaner Production*, 149, 557–568.

Tung, V. C., Allen, M. J., Yang, Y., and Kaner, R. B. (2009). "High-throughput solution processing of large-scale graphene." *Nature Nanotechnology*, 4(1), 25–29.

Ubbrìaco, P., Bruno, P., Traini, A., and Calabrese, D. (2001). "Fly ash reactivity. Formation of hydrate phases." *Journal of Thermal Analysis and Calorimetry*, 66(1), 293–305.

Valenza, J. J., and Scherer, G. W. (2007). "A review of salt scaling: II. Mechanisms." *Cement and Concrete Research*, 37(7), 1022–1034.

Vassilev, S. (2003). "Phase-mineral and chemical composition of coal fly ashes as a basis for their multicomponent utilization. 1. Characterization of feed coals and fly ashes⋆." *Fuel*, 82(14), 1793–1811.

Vassilev, S. V., and Vassileva, C. G. (2005). "Methods for characterization of composition of fly ashes from coal-fired power stations: A critical overview." *Energy & Fuels*, 19(3), 1084–1098.

Vassilev, S. V., Baxter, D., Andersen, L. K., and Vassileva, C. G. (2013). "An overview of the composition and application of biomass ash. Part 1. Phase–mineral and chemical composition and classification." *Fuel*, 105, 40–76.

Vassilev, S. V., Menendez, R., Borrego, A. G., Diaz-Somoano, M., and Rosa Martinez-Tarazona, M. (2004a). "Phase-mineral and chemical composition of coal fly ashes as a basis for their multicomponent utilization. 3. Characterization of magnetic and char concentrates." *Fuel*, 83(11–12), 1563–1583.

Vassilev, S. V., Menendez, R., Diaz-Somoano, M., and Martinez-Tarazona, M. R. (2004b). "Phase-mineral and chemical composition of coal fly ashes as a basis for their multicomponent utilization. 2. Characterization of ceramic cenosphere and salt concentrates." *Fuel*, 83(4–5), 585–603.

Vassilev, S. V., Vassileva, C. G., Karayigit, A. I., Bulut, Y., Alastuey, A., and Querol, X. (2005). "Phase–mineral and chemical composition of composite samples from feed coals, bottom ashes and fly ashes at the Soma power station, Turkey." *International Journal of Coal Geology*, 61(1–2), 35–63.

Velandia, D. F., Lynsdale, C. J., Provis, J. L., Ramirez, F., and Gomez, A. C. (2016). "Evaluation of activated high volume fly ash systems using Na2SO4, lime and quicklime in mortars with high loss on ignition fly ashes." *Construction and Building Materials*, 128, 248–255.

Wallah, S. E., and Rangan, B. V. (2006). *Low-Calcium Fly Ash-Based Geopolymer Concrete: Long-Term Properties*. Curtin University of Technology, Perth, Australia.

Wang, A., Zhang, C., and Sun, W. (2004a). "Fly ash effects: II. The active effect of fly ash." *Cement and Concrete Research*, 34(11), 2057–2060.

Wang, K., Shah, S. P., and Mishulovich, A. (2004b). "Effects of curing temperature and NaOH addition on hydration and strength development of clinker-free CKD-fly ash binders." *Cement and Concrete Research*, 34(2), 299–309.

Wang, P., Wang, J., Qin, Q., and Wang, H. (2017). "Life cycle assessment of magnetized fly-ash compound fertilizer production: A case study in China." *Renewable and Sustainable Energy Reviews*, 73, 706–713.

Wang, Y., Geng, S., Zhao, P., Du, H., He, Y., and Crittenden, J. (2016). "Cost–benefit analysis of GHG emission reduction in waste to energy projects of China under clean development mechanism." *Resources, Conservation and Recycling*, 109, 90–95.

Wardhono, A., Gunasekara, C., Law, D. W., and Setunge, S. (2017). "Comparison of long term performance between alkali activated slag and fly ash geopolymer concretes." *Construction and Building Materials*, 143, 272–279.

Williams, A., Jones, J. M., Ma, L., and Pourkashanian, M. (2012). "Pollutants from the combustion of solid biomass fuels." *Progress in Energy and Combustion Science*, 38(2), 113–137.

Williams, R. P., and van Riessen, A. (2010). "Determination of the reactive component of fly ashes for geopolymer production using XRF and XRD." *Fuel*, 89(12), 3683–3692.

Xu, G., and Shi, X. (2016). "Exploratory Investigation into Upcycling of Coal Fly Ash as Sole Binder for Mortars." *Proceedings of the Transportation Research Board 95th Annual Meeting*, Washington, D.C.

Xu, G., and Shi, X. (2017a). "Graphene oxide modified pervious concrete with fly ash as sole binder." *DEStech Transactions on Engineering and Technology Research*, (ictim).

Xu, G., and Shi, X. (2017b). "Exploratory investigation into a chemically activated fly ash binder for mortars." *Journal of Materials in Civil Engineering*, 29(11), 06017018.

Xu, G., and Shi, X. (2018a). "Impact of chemical deicers on roadway infrastructure: Risks and best management practices." *Sustainable Winter Road Operations*, John Wiley & Sons, Ltd, 211–240.

Xu, G., and Shi, X. (2018b). "Graphene oxide-modified pervious concrete with fly ash as sole binder." *Materials Journal*, 115(3), 369–379.

Xu, G., and Shi, X. (2018c). "Characteristics and applications of fly ash as a sustainable construction material: A state-of-the-art review." *Resources, Conservation and Recycling*, 136, 95–109.

Xu, G., Yang, Z., Dutta, U., Tang, L., and Marx, E. (2011). "Seasonally frozen soil effects on the seismic site response." *Journal of Cold Regions Engineering*, 25(2), 53–70.

Xu, G., Navarro, L. G., Wong, K., and Shi, X. (2017a). "Freeze-Thaw and Salt Resistance of a Fly Ash Based Pervious Concrete." *ACI Fall Convention 2017. ACI Special Publication*.

Xu, G., Sturges, L., Chapman, M., Albrecht, C., Bergner, D., and Shi, X. (2017b). "Snow removal performance metrics." *Transportation Research Record: Journal of the Transportation Research Board*, 2613, 61–70.

Xu, G., Zhong, J., and Shi, X. (2018). "Influence of graphene oxide in a chemically activated fly ash." *Fuel*, 226, 644–657.

Yang, D., Fan, L., Shi, F., Liu, Q., and Wang, Y. (2017). "Comparative study of cement manufacturing with different strength grades using the coupled LCA and partial LCC methods—A case study in China." *Resources, Conservation and Recycling*, 119, 60–68.

Yang, J., Zhao, Y., Zyryanov, V., Zhang, J., and Zheng, C. (2014). "Physical–chemical characteristics and elements enrichment of magnetospheres from coal fly ashes." *Fuel*, 135, 15–26.

Yang, Z., Brown, H., and Cheney, A. (2006). "Influence of moisture conditions on freeze and thaw durability of Portland cement pervious concrete." *Concrete Technology Forum: Focus on Pervious Concrete*, Citeseer, 24–25.

Yang, Z., Dutta, U., Xu, G., Hazirbaba, K., and Marx, E. E. (2011). "Numerical analysis of permafrost effects on the seismic site response." *Soil Dynamics and Earthquake Engineering*, 31(3), 282–290.

Yao, Z. T., Ji, X. S., Sarker, P. K., Tang, J. H., Ge, L. Q., Xia, M. S., and Xi, Y. Q. (2015). “A comprehensive review on the applications of coal fly ash.” *Earth-Science Reviews*, 141, 105–121.

Zhang, Z., Provis, J. L., Reid, A., and Wang, H. (2014). “Fly ash-based geopolymers: The relationship between composition, pore structure and efflorescence.” *Cement and Concrete Research*, 64, 30–41.

Zhuang, X. Y., Chen, L., Komarneni, S., Zhou, C. H., Tong, D. S., Yang, H. M., Yu, W. H., and Wang, H. (2016). “Fly ash-based geopolymer: clean production, properties and applications.” *Journal of Cleaner Production*, 125, 253–267.